J. Phys. A: Math. Gen. **32** (1999) 6791–6820. Printed in the UK PII: S0305-4470(99)03006-1

Spectral statistics in chaotic systems with two identical, connected cells

T Dittrich†‖, G Koboldt‡¶, B Mehlig† and H Schanz§

† Max-Planck-Institut für Physik komplexer Systeme, Nöthnitzer Straße 38, D-01187 Dresden, Germany

‡ Institut für Physik, Universität Augsburg, Memminger Straße 6, D-86135 Augsburg, Germany

§ Max-Planck-Institut für Strömungsforschung, Bunsenstraße 10, D-37073 Göttingen, Germany

Received 24 March 1999, in final form 30 June 1999

Abstract. Chaotic systems that decompose into two cells connected only by a narrow channel exhibit characteristic deviations of their quantum spectral statistics from the canonical random-matrix ensembles. The equilibration between the cells introduces an additional classical timescale that is also manifest in the spectral form factor. If the two cells are related by a spatial symmetry, the spectrum shows doublets, reflected in the form factor as a positive peak around the Heisenberg time. We combine a semiclassical analysis with an independent random-matrix approach to the doublet splittings to obtain the form factor on all time (energy) scales. Its only free parameter is the characteristic exchange time between the cells in units of the Heisenberg time.

1. Introduction

Most of the pioneering enquiries into quantum chaos have been focused on bounded systems—closed billiards, atomic systems—whose classical dynamics knows only a single global timescale defined by, e.g., the inverse Kolmogorov entropy, which describes the ergodic coverage of phase space. The absence of other classical times has facilitated the understanding of quantum-to-classical relationships and has opened the view for universal features in spectra and eigenfunctions of classically chaotic systems.

Extended systems represent another, still simple, extreme. They reach ergodicity only on a timescale that exceeds all other characteristic times. With extended systems, basic solid-state concepts enter quantum chaos. The crucial role of long-range spatial order, in particular, for spectrum and transport has to be considered in the unfamiliar context of dynamical disorder. Using a semiclassical approach, some light was recently shed on the spectral signatures of chaotic diffusion, both in the band structure of periodic systems [1] and in the discrete spectra of disordered systems with localized eigenstates [2–4].

A region intermediate between bound and extended is marked by systems comprising of just a few weakly connected similar cells. In the following, we will consider spatial confinements or phase-space structures that decompose into two compartments, connected only by a 'bottleneck' (figure 1) [5]. Equilibration between the cells then takes much longer than the ergodic coverage of a single cell. It constitutes a second independent timescale of the classical dynamics.

‖ Permanent address: Departamento de Fínodot sica, Universidad de los Andes, A A 4976, Santafé de Bogotá, Colombia.

¶ Present address: Fachbereich 7 – Physik, Universität GHS Essen, D-45117 Essen, Germany.

0305-4470/99/396791+30$30.00

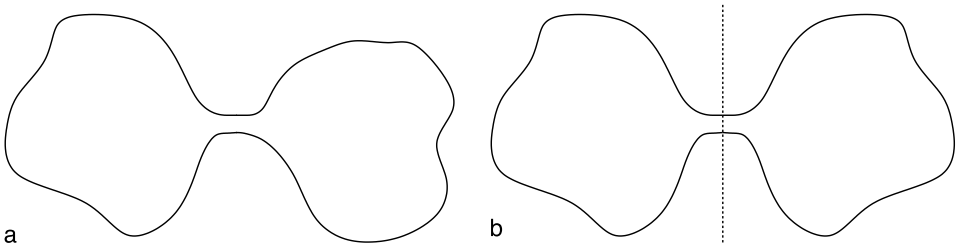

Figure 1. Two-cell billiard with narrow bottleneck, of arbitrary (*a*) and reflection-symmetric shape (*b*).

Chaotic systems with two cells have quite diverse applications. The phase space of alkali atoms in a strong magnetic field may contain two almost disjunct chaotic regions, related by a spatial symmetry [6]. Similar systems arise as models for non-ergodic reaction dynamics in quantum chemistry [7]. More generally, they form prototypes of systems decomposing into two similar, weakly coupled parts. In this sense, they can represent heavy nuclei in a final state of fission [8], or nuclei with their two isospin subsystems interacting weakly due to a slight breaking of isospin invariance [9].

In their quantum mechanical properties, two-cell systems already exhibit the decisive influence of spatial symmetry. If the two cells are of arbitrary shape or size (figure 1(*a*)), their restricted communication will merely be reflected in a quantitative deviation from the canonical random-matrix statistics [5]. It does not introduce any qualitatively new feature. The situation changes considerably if the cells are related by some twofold spatial symmetry (figure 1(*b*)). A genuine quantum phenomenon, a coherent mode of transport between the cells emerges, and the spectrum shows systematic quasidegeneracies. This clustering of levels is manifest in the two-point correlations as a marked *positive* peak on the scale of the mean single-cell level separation, or in the time domain, the single-cell Heisenberg time [1].

This phenomenon should be carefully distinguished from tunnelling. To be sure, the doublets do resemble tunnel splittings in the sense that they are based on a discrete spatial symmetry and correspond to quantum coherent transport on very long timescales. Moreover, in the wavenumber regime where there is no open channel in the constriction between the cells, the wavefunctions decay exponentially into this region. Even at higher wavenumber, the amplitude is often strongly suppressed there (cf figure 6). Since, however, there is neither a potential nor a dynamical barrier involved, this transport is slow but not classically forbidden.

Chaos-assisted tunnelling, in contrast, is a hallmark of bistable systems with a mixed phase space [10, 12, 13]. It occurs between symmetry-related pairs of *regular* islands in phase space that are separated by a chaotic region. Here, in contrast, we are dealing with symmetry-related *chaotic* regions communicating through a narrow bridge in space. Still, a similar situation can also occur in mixed bistable systems. In fact, the distribution of the splittings of doublet states supported by symmetry-related pairs of chaotic regions [14] forms an important input to the distribution of tunnel splittings in chaos-assisted tunnelling [15].

In the following sections, we develop a theory for the spectral statistics of two-cell systems that rests largely on recent progress in the analysis of band structures of classically chaotic systems with spatial periodicity [1]. There, an important input has been the notion of form factors with a winding-number argument, specific for transitions spanning a corresponding number of unit cells. Likewise, the group property of a reflection or translation symmetry of a two-cell system enables the definition of form factors with a rudimentary spatial resolution, expressed by a binary index that indicates either return to the same cell or transport into the

opposite cell.

However, compared with [1], we not only go from a large value of N, the number of unit cells, to $N = 2$. Here, we shall concentrate on the case of slow exchange between the cells, the 'weak-coupling' or 'tight-binding' limit in solid-state terminology, while [1] was devoted to the opposite case. This implies that, even if the two-cell system is 'unfolded' to form an infinite chain (see appendix A), the concept of homogeneous diffusion no longer applies. Rather, in the unfolded picture, we are dealing with a spatially discrete diffusion process that deviates significantly, on short timescales, from ordinary diffusion. Concerning the spectral statistics, the principal consequence is that we are now dealing with *flat* 'bands'.

In order to extend a semiclassical treatment of the spectral correlations to energy scales below the mean level spacing, information on the spreading of the possibly complex trajectories that mediate the long-time transitions [14, 16], analogous to the sum rules for ergodicity [17] or diffusion [2, 3], would be required. Alternatively, we would have to surmount the diagonal approximation. We circumvent this open problem and adopt a different strategy. In the spirit of Berry's semiclassical approximation for the form factors of random-matrix ensembles [18], we impose plausible assumptions on the distribution of the narrow splittings. They are based on the relation of the doublet splittings in two-cell compounds to the resonance widths in corresponding single-cell systems, obtained by opening up the system at the constriction. We derive this relation in the case of a single open channel between the cells, where doublet splittings and resonance widths are not simply identical.

Switching back from the distribution of doublet splittings to the corresponding time-domain function valid on long timescales, we match the resulting long-time asymptote with the semiclassical short-time behaviour. In this way, we achieve expressions for the spectral two-point correlations on all timescales. They are universal in that they contain, as the only free parameter, the characteristic time for equilibration between the cells. It is the two-cell analogue of the conductance, the scaling parameter in the case of long chains.

We introduce the classical concepts relevant for the dynamics of systems with two identical, connected cells in section 2. In section 3, we define form factors specific for an element of the symmetry group of the system. A semiclassical theory for the short-time regime of these form factors is developed in section 4, while section 5 is devoted to their quantum long-time behaviour. Some of these calculations are extended to the case of unrestricted values of N in two of the appendices. Section 6 serves to introduce four illustrative models: two versions of a Sinai billiard [19, 20], quantum graphs [21] configured in such a way that they form a two-cell system, a two-cell variant of the quantum kicked rotor [1, 22], and a random-matrix model [11, 12]. Spectral data obtained numerically for these models corroborate our theory. Section 7 contains a synopsis of the various limiting cases covered in this paper.

2. Classical dynamics in two-cell systems

As a minimal version of a classical two-cell system, consider the following model: two spatially confined compartments are connected by some narrow duct (figure 1(*a*)). In view of the intended applications, we require a few additional properties. The leakage from the cell where the system is prepared (subscript '0' in the following) to the opposite side (subscript '1') should be completely described by a single timescale $1/\lambda$. This amounts to an exponential decay of the population from the initial cell, if it were opened by removing the opposite cell. We require the rate λ to be the same in both directions. A sufficient condition for this to be true is that the cells form a (translation- or reflection-) symmetric pair (figure 1(*b*)). Finally, we assume that the dynamics within the cells is chaotic and thus ergodic, and that coverage of a single cell is reached instantaneously on the scale $1/\lambda$.

Under these conditions, the time evolution of the probability to stay in either cell obeys the following pair of simple master equations:

$$\begin{aligned} \dot{P}_0(t) &= \lambda(P_1(t) - P_0(t)) \\ \dot{P}_1(t) &= \lambda(P_0(t) - P_1(t)). \end{aligned} \tag{1}$$

The relaxation into equilibrium of the two probabilities, given by $\lim_{t\to\infty} P_{0/1}(t)/(P_0(t) + P_1(t)) = \frac{1}{2}$, is governed by the rate $\Lambda = 2\lambda$. From an initial state $P_0(0) = 1$, $P_1(0) = 0$, they evolve as

$$P_{0/1}(t) = \tfrac{1}{2}(1 \pm \mathrm{e}^{-\Lambda t}). \tag{2}$$

The population difference

$$P_{\mathrm{d}}(t) = P_0(t) - P_1(t) \tag{3}$$

is another relevant quantity. Besides the sum $P_0(t) + P_1(t)$, it plays the rôle of an eigenmode amplitude of the master equations (1). Its time evolution reads, for the same initial state as above,

$$P_{\mathrm{d}}(t) = \mathrm{e}^{-\Lambda t}. \tag{4}$$

The above considerations also apply if the cells communicate through two or more physical channels. This includes, in particular, the case of two cells connected at both 'ends' to form a ring. The rates of probability exchange through the channels then just add to give the global rate λ. The diffusive dynamics that results if a two-cell ring configuration is unrolled into an infinite chain, is discussed in appendix A.

As an example, we state the explicit expression for the decay rate λ in the case of an ergodic double billiard as in figure 1. The phase-space area leaving one cell of the billiard in time $\mathrm{d}t$ through the connecting channel of width s, at unit speed, is $\mathrm{d}\Omega = 2s\mathrm{d}t$. This is to be normalized by the area A of a cell and by 2π, the size of momentum space projected onto the energy shell. The resulting approximation for the escape rate is [23]

$$\lambda_{\mathrm{erg}} = \frac{s}{\pi A}. \tag{5}$$

3. Generalized form factors

In quantum systems, each unitary symmetry gives rise to a constant of the motion, a 'good quantum number'. It takes as many values as there are irreducible representations of the symmetry, and the full spectrum can be decomposed into subspectra, each of which pertains to a given irreducible representation. Formally, the decomposition is effected by the projectors [24] $\hat{P}_\nu = N^{-1}\sum_{n=0}^{N-1} \chi_\nu(g_n)\hat{U}^\dagger(g_n)$, $\nu = 0, \ldots, N-1$. Here, N is the number of elements g_n of the symmetry group and simultaneously, the number of its representations (for simplicity, we assume all representations to be one dimensional). The character of g_n in the νth representation is referred to as $\chi_\nu(g_n)$, and $\hat{U}(g_n)$ denotes the unitary transformation corresponding to g_n. Spectral densities and correlation functions within a given representation can then be defined on the basis of the symmetry-projected Green function $\hat{G}_\nu(E) = \hat{P}_\nu\hat{G}(E)$, with $\hat{G}(E)$, the Green function for the entire spectrum. For example, the symmetry-projected spectral density in the νth representation is defined as

$$\tilde{d}_\nu(E) = \sum_\alpha \delta(E - E_{\alpha,\nu}) = -\frac{1}{\pi}\mathrm{Im\ tr}[\hat{G}_\nu(E)] \tag{6}$$

where the $E_{\alpha,\nu}$ are the eigenenergies in the νth representation.

For the study of quasidegenerate doublets, another type of spectral density is as relevant as the symmetry-projected one. As an alternative to $\tilde{d}_\nu(E)$, one may define densities and derived quantities that refer to a group element g_n, instead of an irreducible representation ν. The symmetry group induces a tiling of (phase) space, i.e., a decomposition into disjunct segments such that each of them is mapped onto all the others by the transformations in the group, thus covering the entire space [25]. A group-element-specific spectral density therefore provides a rudimentary spatial resolution on the scale of the fundamental domain of the group.

If all representations are one-dimensional, the set of columns of the matrix $\chi_{\nu,n} = \chi_\nu(g_n)$ of group characters forms an orthogonal basis in N dimensions [24]. The same is true for the rows. Therefore, the matrix as a whole has full rank and is invertible. We refer to the inverse matrix as χ^{-1}. Multiplying the vector of symmetry-reduced spectral densities $\tilde{d}_\nu(E)$, equation (6), from the left by χ^{-1}, we obtain the spectral densities [1]

$$d_n(E) = \sum_{\nu=0}^{N-1} (\chi^{-1})_{\nu,n} \tilde{d}_\nu(E) \tag{7}$$

$$= -\frac{1}{\pi} \mathrm{Im} \int_{\mathrm{fd}} \mathrm{d}q\, \hat{G}(g_n(\boldsymbol{q}), \boldsymbol{q}; E). \tag{8}$$

The space integral in equation (8) only extends over the fundamental domain (subscript 'fd') of the tesselated space. The first argument of the Green function in the third line is the image of its second argument, $\boldsymbol{q}$, under g_n. This suggests that $d_n(E)$ refers to transitions from any segment to its image under g_n.

By Fourier transforming equation (7) with respect to energy, we arrive at the analogous density in the time domain,

$$a_n(\tau) = \langle d_{\mathrm{fd}} \rangle^{-1} \int_{-\infty}^{\infty} \mathrm{d}r\, \mathrm{e}^{-2\pi \mathrm{i} r\tau} d_n(r/\langle d_{\mathrm{fd}} \rangle) \tag{9}$$

$$= \int_{\mathrm{fd}} \mathrm{d}q\, \langle g_n(\boldsymbol{q}) | \hat{U}(t_{\mathrm{H}}\tau) | \boldsymbol{q} \rangle. \tag{10}$$

We have switched to dimensionless energy, $r = \langle d_{\mathrm{fd}} \rangle E$, and time, $\tau = t/t_{\mathrm{H}}$, by scaling with the mean spectral density $\langle d_{\mathrm{fd}} \rangle$ in the symmetry-reduced space, and the corresponding Heisenberg time $t_{\mathrm{H}} = 2\pi\hbar\langle d_{\mathrm{fd}} \rangle$, respectively. Note that we restrict ourselves to leading semiclassical order such that the mean spectral density $\langle d_{\mathrm{fd}} \rangle$ does not depend on the irreducible representation ν. Equation (10) describes an amplitude to return modulo the symmetry transformation g_n. The corresponding return probability is given by the form factor

$$K_n(\tau) = \frac{1}{\Delta r_{\mathrm{fd}}} |a_n(\tau)|^2 \tag{11}$$

where Δr_{fd} is the total width, in units of $\langle d_{\mathrm{fd}} \rangle$, of the spectrum considered.

In (9) we have assumed that an arbitrarily large spectral window can be used for the computation of $a_n(\tau)$. In this case, equation (11) is exactly equivalent to a definition of the form factor as the Fourier transform of a spectral autocorrelation function according to the Wiener–Khintchin theorem. In numerical computations this relation holds approximately provided that $1 \ll \Delta r$. In this limit, the result also does not depend on the form of the window function used to truncate the spectrum. On the other hand, the spectral window must be chosen small with respect to classical energy scales in order to allow for a meaningful semiclassical description. Definitions of form factors for finite spectral segments, other than equations (9) and (11), e.g., truncating directly the two-point correlations and not the density, are conceivable but inappropriate for our purposes. These practical aspects of the computation are discussed in [1, 3]. We shall give more details of the computation of the form factors in section 6, in the context of the respective models to which they apply.

For a two-cell system, a symmetry that maps one cell to the other can be a reflection or a translation. Their group elements are identity (denoted by $n = 0$ in the following) and reflection or translation ($n = 1$, without distinguishing the two). The characters are both 1 in the symmetric (subscript '+') representation, and ± 1 in the antisymmetric ('$-$') representation. Following the general discussion above, we define symmetric and antisymmetric form factors, respectively, by

$$\tilde{K}_{\pm}(\tau) = \frac{1}{\Delta r_{\mathrm{fd}}} |\tilde{a}_{\pm}(\tau)|^2. \tag{12}$$

The amplitudes $\tilde{a}_{\pm}(\tau)$ are obtained, for example, by sorting the spectral data of the two-cell system according to the symmetry of the corresponding eigenstates, and Fourier transforming as in equation (9). Alternatively, $\tilde{K}_{\pm}$ can be interpreted as the form factors of a single cell with Neumann or Dirichlet boundary conditions, respectively, imposed on the line(s) in configuration space common to the two cells. In general, this choice of boundary conditions does not affect the chaoticity of the classical dynamics. Hence we expect the form factor of a single cell to equal the random-matrix result [26] up to normalization, i.e.,

$$\tilde{K}_{\pm}(\tau) = \tfrac{1}{2} K_{\mathrm{RMT}}(\tau). \tag{13}$$

Form factors specific for return to the initial (subscript '0') or switching to the opposite cell ('1') are defined according to equation (7) and equations (9), (11) as

$$K_{0/1}(\tau) = \frac{1}{\Delta r_{\mathrm{fd}}} |\tilde{a}_{+}(\tau) \pm \tilde{a}_{-}(\tau)|^2. \tag{14}$$

Note that the amplitudes are superposed *before* squaring. In section 5 we show that considering the *incoherent* superpositions $K_0(\tau) \pm K_1(\tau)$, in turn, provides an approximate access to the distribution of doublet splittings and inter-doublet separations, respectively.

The combination of amplitudes $\tilde{a}_{+}(\tau) + \tilde{a}_{-}(\tau)$ entering $K_0(\tau)$ in equation (14) is obtained in (9), when d_n on the rhs is replaced by the total spectral density of the two-cell system. Hence K_0 is—up to scaling of time and energy—equivalent to a form factor defined without any reference to the spatial symmetry of the two cells.

In equations (12) and (14) we have chosen a normalization which ensures that $\tilde{K}_{\pm}(\tau)$ and $K_{0/1}(\tau)$ approach the same value $\frac{1}{2}$ for $\tau \to \infty$, provided the two cells are not completely disconnected. In addition, the sums of the symmetry-projected and the group-element-specific form factors are the same for arbitrary time τ,

$$K_0(\tau) + K_1(\tau) = \tilde{K}_{+}(\tau) + \tilde{K}_{-}(\tau). \tag{15}$$

This identity may be interpreted as a preservation of norm and follows generally from the unitarity of the matrix $\chi_{\nu,n}$ of group characters. Due to (13) it leads to the relation

$$K_0(\tau) + K_1(\tau) = K_{\mathrm{RMT}}(\tau). \tag{16}$$

It is instructive at this stage, to consider the trivial limiting cases of two completely isolated or two very strongly interacting cells, respectively. In the first case, we have from the definitions (7), (9) and (14) $K_1(\tau) = 0$. Then (13) implies $K_0(\tau) = K_{\mathrm{RMT}}(\tau)$, and this is indeed what is expected within our scaling of time and energy from the fact that the total spectrum is the superposition of two *identical* random-matrix spectra. In the other extreme, the two subspectra of positive and negative parity can be considered statistically independent, which has the consequence $K_0(\tau) = K_1(\tau) = K_{\mathrm{RMT}}(\tau)/2$.

4. Semiclassical regime

In order to construct a semiclassical trace formula for the symmetry-projected spectral density $\tilde{d}_\nu(E)$, equation (6), the concept of periodic orbits has to be extended [25]. In case the dynamics within the cells has no significant admixture of regular motion, the trace formula reads

$$\tilde{d}_\nu^{(\mathrm{sc})}(E) = \frac{1}{\mathrm{i}\hbar N} \sum_j \frac{T_j^{(\mathrm{p})}}{\kappa_j \sqrt{|\det(M_j - I)|}} \chi_\nu(g_j) \exp\left(\mathrm{i}\frac{S_j}{\hbar} - \mathrm{i}\mu_j \frac{\pi}{2}\right). \tag{17}$$

The sum now runs over generalized period orbits j. Their end point is not necessarily identical with the starting point, but must be mapped to it by some group element g_j. The corresponding term in equation (17) then contains the character $\chi_\nu(g_j)$ as an extra, non-classical phase factor. A correction of the amplitude for orbits that coincide with symmetry lines is effected by κ_j [25]. As usual, $T_j^{(\mathrm{p})}$, M_j, S_j, μ_j denote primitive period, stability matrix, classical action, and Maslov index, respectively, of orbit j.

The rôle of the generalized periodic orbits becomes even more transparent in the analogous trace formula for the group-element-specific density,

$$d_n^{(\mathrm{sc})}(E) = \frac{1}{\mathrm{i}\hbar N} \sum_j \frac{T_j^{(\mathrm{p})}}{\kappa_j \sqrt{|\det(M_j - I)|}} \delta(g_j, g_n) \exp\left(\mathrm{i}\frac{S_j}{\hbar} - \mathrm{i}\mu_j \frac{\pi}{2}\right). \tag{18}$$

The delta function in the second line equals unity if its arguments coincide and vanishes otherwise. It selects orbits j whose endpoints are connected by g_n. They mediate transport from the original segment to its image, with the restriction that initial and final points are exactly related by the symmetry.

The interpretation that spectral quantities associated with g_n describe transport from an original space segment to its image under g_n is borne out quite explicitly by the form factors. A semiclassical expression for the $K_n(\tau)$ can be derived by substituting into equation (11) the trace formula (18), Fourier transformed to the time domain as in equation (9). Within the diagonal approximation with respect to pairs of generalized periodic orbits [1–4, 18], which is valid for times $t \ll t_\mathrm{H}$, one obtains,

$$K_n^{(\mathrm{sc})}(\tau) = \gamma_n \tau P(g_n, \tau t_\mathrm{H}) \qquad \tau \ll 1. \tag{19}$$

Equation (19) relates the form factors to the classical probability $P(g_n, t)$ to return in time t to a phase-space point related to the starting point by g_n. The contribution of repetitions of shorter periodic orbits has been neglected in equation (19). By introducing a global degeneracy factor γ_n to account for antiunitary symmetries such as time-reversal invariance, we ignored the occurrence of self-retracing orbits. This factor takes the value 2 if orbits that are periodic modulo g_n are generically time-reversal degenerate, and 1 otherwise. A non-trivial dependence of γ_n on n can occur, e.g., in periodic systems with $N \geqslant 3$ unit cells [1]. There, time-reversal invariance is generally broken for orbits with winding numbers n mod $N \neq 0$, $N/2$, due to Bloch phases that are not real.

In the spirit of the known classical sum rules for ergodic systems [17], we assume that the generalized periodic orbits are not distinct from the generic non-periodic ones in their average spreading. We can then relate the $P(g_n, t)$ to the classical propagator $p(\boldsymbol{r}', \boldsymbol{r}; t)$ (the integral kernel of the Frobenius–Perron operator) by a phase-space integration over the fundamental domain,

$$P(g_n, t) = \int_\mathrm{fd} \mathrm{d}r \; p(g_n(\boldsymbol{r}), \boldsymbol{r}; t) \tag{20}$$

where $\boldsymbol{r} = (\boldsymbol{p}, \boldsymbol{q})$ denotes a phase-space point within the fundamental domain on the energy shell. In case that the chaotic coverage of the single cells is homogeneous, the classical

propagator depends on g_n but not on $\boldsymbol{r}$ and can thus be expressed by the coarse-grained probabilities defined in section 2 [1]. In this case the integration in equation (20) becomes trivial and results in

$$P(g_n, t) = P_n(t). \tag{21}$$

For the group-element-specific form factors defined for two-cell systems, equation (14), the semiclassical expression finally reads

$$K_{0/1}^{(\mathrm{sc})}(\tau) = \gamma\tau P_{0/1}(\tau t_{\mathrm{H}}) \tag{22}$$

$$= \frac{\gamma\tau}{2}(1 \pm \mathrm{e}^{-2\lambda t_{\mathrm{H}}\tau}) \qquad \tau \ll 1. \tag{23}$$

Here we have used the fact that in symmetric two-cell systems, the degeneracy factor γ does not depend on g_n.

A detailed investigation of the phase-space coverage for a specific double billiard [29] shows that—for a finite time depending on the special properties of the employed model—there can be small deviations from the homogeneity assumed in the derivation of equation (22). Similar restrictions of our theory may arise from the neglect of marginally stable (bouncing-ball) orbits. However, all the approximations discussed so far are standard within a semiclassical theory for two-point correlations, and although they cannot be rigorously justified, they are sufficient to reproduce most of the available numerical data [1–4, 18].

The most important limitation in this respect is due to the diagonal approximation for systems with time-reversal invariance, $\gamma = 2$. It is well known that this approximation only reproduces the slope near $\tau = 0$ for systems with a single chaotic cell, and it is not surprising that we observe the same for a two-cell system when we compare (23) with equation (16). The semiclassical result deviates exactly by the same factor $\gamma\tau/K_{\mathrm{RMT}}(\tau)$ known from simple ergodic systems [18].

In the remaining paragraphs of this section, we briefly discuss the influence of a small breaking of the symmetry of the two billiard cells. It is clear that the overshoot of $K_0(\tau)$ over its asymptotic value, as described by equation (23), is the result of the symmetry. For an asymmetric double billiard, this overshoot should vanish altogether, leaving the steeper initial rise of the form factor implied by equation (23) as the only spectral signature of the restricted exchange between the cells. However, we expect that there exists a continuous crossover, as a function of some parameter, that expresses the degree of symmetry breaking.

A semiclassical approach that extends the above arguments to the case of a weakly broken symmetry has been presented in [36]. It is based on the idea that the contributions of a given set of N symmetry-related periodic orbits to the form factor will no longer be N-fold degenerate, but can still be completely included, without resorting to a diagonal approximation within this set. The following assumptions have to be made to justify this strategy: (i), the perturbation is sufficiently weak not to destroy the structural stability of the periodic orbits, i.e., no periodic orbits disappear or are created, as compared with the unperturbed system; (ii), only the change, ΔS, in action has to be taken into account because it appears in the exponential, while the changes in amplitude and period can be neglected; (iii), the changes in action result from many statistically independent perturbations of the orbit so that, by the central limit theorem, they can be considered as Gaussian random variables with zero mean and variance

$$\langle(\Delta S)^2\rangle = \delta^2\tau. \tag{24}$$

The constant δ will serve as the basic parameter for the degree of symmetry breaking. The proportionality to time reflects the accumulation of squared action changes over the length of the periodic orbit.

Under these assumptions, the influence of symmetry breaking can be expressed as an effective degeneracy relating the form factor for broken symmetry to the corresponding one for the symmetric system (in the present context, we are left with the 'symmetry-insensitive' $K_0(\tau)$). For a two-cell system, we find

$$K_0^{(\mathrm{asym})}(\tau,\delta) = \tfrac{1}{2}(1+\mathrm{e}^{-\delta^2\tau})K_0(\tau). \tag{25}$$

Inserting $K_0^{(\mathrm{sc})}(\tau)$ from equation (23), this implies

$$K_0^{(\mathrm{asym})}(\tau,\delta) = \tfrac{1}{2}(1+\mathrm{e}^{-\delta^2\tau})(1+\mathrm{e}^{-2\lambda t_{\mathrm{H}}\tau}). \tag{26}$$

Since this result involves the same semiclassical approximations as we made in the derivation of $K_0^{(\mathrm{sc})}(\tau)$, its validity is likewise restricted to the short-time regime $\tau \ll 1$. Within this regime, it provides the sought interpolation between the symmetric limit, $\delta^2 \ll 1$, and the limit of totally broken symmetry, $\delta^2 \gtrsim 1$. Due to the assumptions enumerated above, in particular that of structural stability, we expect equation (25) to also become unreliable in the latter limit.

5. Long-time regime

In the semiclassical time range, we succeeded in expressing the form factors for all parameter regimes, from two-cell systems without significant separation of the cells to pairs of nearly uncoupled cells, by a single expression, equation (23). We cannot achieve this generality for the regime of long times $t \gtrsim t_{\mathrm{H}}$. The case of weakly coupled ($\lambda t_{\mathrm{H}} \ll 1$) symmetric billiards, to be considered here, requires additional input besides the classical information contained in equation (23). At the same time, this is the most interesting situation because only here do quasidegenerate doublets occur with a splitting much smaller than their typical separation.

As a starting point for an alternative approach valid in the long-time regime, we return to the exact definition of the group-element-specific amplitudes $a_{0/1}(\tau)$. Specializing equation (9) to the two-cell case and inserting the definition (6) of $d_{0/1}(E)$, we obtain

$$a_n(\tau) = \tfrac{1}{2}\sum_{\nu=0}^{1}\mathrm{e}^{\pi\mathrm{i}n\nu}\sum_{\alpha=1}^{N_{\mathrm{d}}}\mathrm{e}^{-2\pi\mathrm{i}\tau r_{\alpha,\nu}} \qquad n=0,1. \tag{27}$$

Here, N_{d} is the number of doublets in the spectrum, i.e., half the total number of levels. We have used the fact that the inverse characters for the twofold reflection or translation group can be concisely written as $(\chi^{-1})_{\nu,n} = \mathrm{e}^{\pi\mathrm{i}n\nu}$, with $\nu = 0, 1$, corresponding to the symmetric and the antisymmetric representations, respectively. In these representations, returning to the symbols '+' and '−', $r_{\alpha,0/1} = r_{\alpha,\pm} = \langle d_{\mathrm{fd}}\rangle E_{\alpha,\pm}$ denote the scaled eigenenergies.

We introduce the concept of doublets by writing the eigenenergies as

$$r_{\alpha,\pm} = R_\alpha \pm r_\alpha. \tag{28}$$

The long-time limit of the form factors for the canonical random-matrix ensembles is usually derived under the assumption that the full phases τr are random for $\tau \gg 1$. Likewise, here we assume the analogous phases τR_α contributed by the doublet midpoints to be random in the long-time limit. Upon squaring the amplitudes $\tilde{a}_\pm(\tau)$ to obtain the corresponding form factors, this amounts to a diagonal approximation with respect to the index α,

$$K_{0/1}(\tau) = \frac{1}{2} \pm \frac{1}{2N_{\mathrm{d}}}\sum_{\alpha=1}^{N_{\mathrm{d}}}\cos(4\pi\tau r_\alpha). \tag{29}$$

In fact, equation (29) can also be derived if the two-cell system is unrolled to an infinite chain and the doublets are considered as points of continuous bands, see appendix B.

If $N_{\rm d}$ is sufficiently large, we can replace the sum over α by an integral and consider the integration as a Fourier transformation, to obtain

$$K_{0/1}(\tau) = \tfrac{1}{2}(1 \pm p_{\rm d}(2\tau)) \tag{30}$$

with

$$p_{\rm d}(\tau) = \int_0^\infty {\rm d}r\ \cos(2\pi r\tau)\, p_{\rm d}(r). \tag{31}$$

This is the Fourier transform of the distribution of doublet splittings

$$p_{\rm d}(r) = \sum_{\alpha=1}^{N_{\rm d}} \delta(r - |r_{\alpha,-} - r_{\alpha,+}|). \tag{32}$$

Forming the difference of the two form factors,

$$p_{\rm d}(\tau) = K_0(\tau/2) - K_1(\tau/2) \tag{33}$$

we see that this equals the time-domain splitting distribution in its long-time, or equivalently, low-energy limit. Given that the form factors contain information merely on two-point correlations irrespective of symmetry, it is actually surprising that they can be related, as in equation (33), to a quantity that requires an unambiguous identification of doublets. This can be explained by the fact that we had to assume in the derivation that the midpoints R_α of the doublets are statistically independent of their splittings r_α, which requires a clear separation of scales between splittings and spacings of doublets. Indeed, equation (33) ceases to be valid for $\tau \lesssim 1$, corresponding to the regime of large $r_\alpha \gtrsim 1$.

We do not have any semiclassical access to $p_{\rm d}(r)$. Nevertheless, in order to make some progress, we shall resort to results of random-matrix theory on the distribution of resonance widths, and argue that the doublet splittings obey a similar distribution.

Suppose the channel between the two cells to be replaced by a semi-infinite duct of constant width, so that two single cells remain, each with a small opening that couples its interior to the continuum in the duct. This situation is illustrated with a symmetric two-cell billiard in figure 2. The spectra of the open single cells will then exhibit narrow resonances at roughly the same energies where the corresponding closed two-cell system shows doublets. It is plausible that the doublet splittings of the two-cell configuration are related to the resonance widths in the single-cell setup, at least in a statistical sense. Indeed, this assumption is often made, e.g., in nuclear theory, and supported by semiclassical and random-matrix arguments. In short, it is justified by the fact that both quantities, widths and splittings, can be expressed by the same wavefunction overlaps and should therefore obey the same distribution.

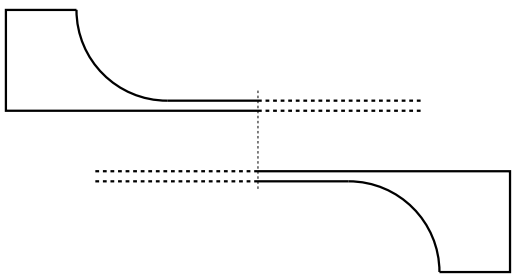

Figure 2. Two identical scattering systems are obtained when the channel connecting the two halves of a symmetric two-cell billiard is replaced by a semi-infinite waveguide of constant width. We argue that small doublet splittings between states of the two-cell billiard correspond to narrow resonances of the corresponding pair of scattering systems (see text).

Here we are interested in the case of very few open channels in the connecting section, since this is required for the formation of narrow doublets. In this limit, we cannot expect random-matrix theory to remain valid. However, taking the point of view of the scattering approach to quantization [27], we show in the following paragraphs that there is still a close relation, though not an exact identity, between the respective distributions of widths and splittings.

We shall specifically consider the wavenumber regime where there is just a single open channel in the connecting section. This case is realized in the majority of the numerical examples below. Here, the calculation is particularly straightforward and transparent, because the scattering in the cell is described by a 1×1 scattering 'matrix' (since there is only one opening, all incoming waves leave as reflected waves). As we are interested in isolated narrow resonances, we assume their widths to be small compared with their separations. The S matrix can then be written in the form

$$S(r) = \mathrm{e}^{\mathrm{i}\theta} \frac{r - r_0 - \mathrm{i}g}{r - r_0 + \mathrm{i}g} \tag{34}$$

where $r_0 - \mathrm{i}g$ denotes the position of the resonance pole in the complex energy plane, again in units of the mean level spacing. The quantization condition in terms of $S(r)$ is [27]

$$S(r_\pm) = \pm 1 \tag{35}$$

the upper sign referring to the case of symmetric states (subscript '+'), the lower one to antisymmetric states ('$-$'). Inserting equation (34) gives the eigenvalues

$$r_+(\theta) = r_0 + g \cot \theta/2 \tag{36}$$

$$r_-(\theta) = r_0 - g \tan \theta/2 \tag{37}$$

for the symmetric and antisymmetric cases, respectively, separated by the splitting

$$r(\theta) = |r_-(\theta) - r_+(\theta)| = \frac{2g}{|\sin \theta|}. \tag{38}$$

This function is π periodic. In the interval $0 \leqslant \theta < \pi$, it has a minimum at $\theta = \pi/2$, with a functional value $r(\pi/2) = 2g$. It diverges at $\theta = 0, \pi$.

This analysis already exhibits the essential facts to be demonstrated: there is a connection between resonance widths and doublet splittings, but it depends on the unknown value of the total phase θ of the S matrix. As no value of θ is singled out *a priori*, we assume equidistribution of the total phase. Under this condition, the main contribution to the distribution of the splittings comes from $r \gtrsim 2g$. This is the simple relation between doublet splittings and resonance widths we seek. Quantitatively, we find the probability density

$$p_\mathrm{d}(r|g) = \frac{4g}{\pi r^2} \left(1 - \left(\frac{2g}{r}\right)^2\right)^{-1/2} \qquad (r \geqslant 2g) \tag{39}$$

for the splittings. It is normalized to unity, but its first moment already diverges. Indeed, as we started from the assumption of small splittings, we cannot expect the result to be valid for large splittings. The missing cutoff will be given by our semiclassical considerations which cover the complementary regime of large splittings.

The distributions of wavefunction amplitudes and of resonance widths are among the established principal results of random-matrix theory [28]. Even if details of their application to quantum chaotic scattering are still under study, we can, for the present purposes, adopt the canonical random-matrix results for $p(g)$, the probability density of the resonance widths, and substitute them to obtain the unconditional splitting distribution $p_\mathrm{d}(r)$.

Its general relation with the conditional $p_\mathrm{d}(r|g)$ and $p(g)$ reads

$$p_\mathrm{d}(r) = \int_0^\infty \mathrm{d}g \; p(g) p_\mathrm{d}(r|g). \tag{40}$$

In order to return from the energy to the time domain, we perform a Fourier transformation of $p_{\rm d}(r)$, cf equation (31). Inserting the explicit expression (39) for $p_{\rm d}(r|g)$, we obtain

$$p_{\rm d}(\tau) = \frac{1}{\pi}\int_0^1 {\rm d}x\, \frac{2}{\sqrt{1-x^2}}\, p\left(\frac{2\tau}{x}\right) \tag{41}$$

where $p(\tau) = \int_0^\infty {\rm d}g\, \cos(2\pi g\tau)\, p(g)$, in turn, is the Fourier transform of the distribution of resonance widths.

For time-reversal-invariant systems, the resonance widths obey a Porter–Thomas distribution [28]

$$p_{\rm PT}(g) = \frac{{\rm e}^{-g/2\langle g\rangle}}{\sqrt{2\pi\langle g\rangle g}}. \tag{42}$$

The integral obtained by inserting the Fourier transform

$$p_{\rm PT}(\tau) = \sqrt{\frac{1+\sqrt{1+[4\pi\langle g\rangle\tau]^2}}{2(1+[4\pi\langle g\rangle\tau]^2)}} \tag{43}$$

into (41) can be used for a numerical computation of the form factor. In the long-time limit, from an asymptotic expansion of (43) we find

$$p_{\rm d}(\tau) = \frac{1}{4\pi}\frac{\Gamma(\frac{3}{4})}{\Gamma(\frac{5}{4})}\frac{1}{\sqrt{\langle g\rangle\tau}} + {\rm O}((\langle g\rangle\tau)^{-3/2}). \tag{44}$$

If time-reversal invariance is broken, the resonance widths are exponentially distributed,

$$p_{\rm exp}(g) = \frac{1}{\langle g\rangle}{\rm e}^{-g/\langle g\rangle} \tag{45}$$

$$p_{\rm exp}(\tau) = \frac{1}{1+(2\pi\langle g\rangle\tau)^2} \tag{46}$$

and accordingly

$$p_{\rm d}(\tau) = \frac{1}{1+4\pi\langle g\rangle\tau\sqrt{1+(4\pi\langle g\rangle\tau)^2}+(4\pi\langle g\rangle\tau)^2}. \tag{47}$$

For $\langle g\rangle\tau \gg 1$ we find $p_{\rm d}(\tau) \to (4\pi\langle g\rangle\tau)^{-2}/2$.

Note that, for both the exponential and Porter–Thomas distributions, the asymptotic behaviour of the doublet splittings for large time/small energy is equivalent to the corresponding resonance-width distribution up to a constant prefactor which relates the mean doublet splitting to $\langle g\rangle$. This constant—it equals $2\pi\Gamma^2(\frac{5}{4})/\Gamma^2(\frac{3}{4}) \approx 3.44$ with and $\sqrt{8} \approx 2.82$ without time-reversal invariance—is somewhat above 2 as anticipated from equation (38).

In figure 3, we compare the Fourier-transformed unconditional splitting distribution equation (41) in the presence and absence of time-reversal invariance with the corresponding distribution of resonance widths for $\langle g\rangle = 0.1$. We see that for $\langle g\rangle\tau \gtrsim 1$, the deviation between the two is not dramatic and conclude that the resonance distribution $p(g)$, Porter–Thomas or exponential, is the crucial input for $p_{\rm d}(\tau)$, while it is quite robust against changes and approximations entering via $p_{\rm d}(r|g)$.

Now we return to our main line of reasoning and attempt a matching of the short-time (large-separation) with the long-time (small-splitting) regime of the form factors. This will simultaneously allow us to calibrate the as yet undetermined parameter $\langle g\rangle$ of the resonance distribution with respect to the classical decay rate λ. We present this calculation only for the simpler case of broken time-reversal invariance. If time-reversal symmetry is obeyed, the bad performance of the diagonal approximation at the Heisenberg time makes an analogous

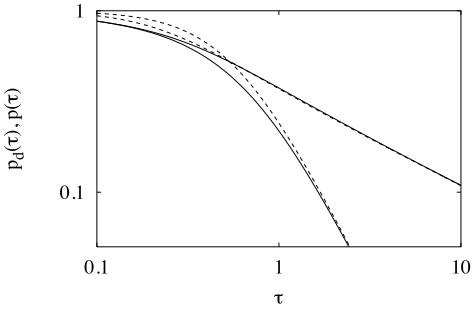

Figure 3. Time-domain splitting distribution equation (41) for symmetric two-cell systems with a single open channel in the connector, in the presence of time-reversal invariance (upper solid curve) and in its absence (lower solid curve). For comparison, the broken curves show the Fourier transforms of the corresponding resonance distributions, i.e., of the Porter–Thomas distribution equation (43), above, and of the exponential distribution equation (46), below. The parameter value common to all curves is $\langle g \rangle = 0.1$.

procedure more problematic. We will discuss this in connection with our numerical results in sections 6.2 and 6.3.

From the semiclassical side, equation (23), we find at the matching point $\tau = 1$,

$$K_{0/1}(1) = \tfrac{1}{2}(1 \pm \mathrm{e}^{-2\lambda t_{\mathrm{H}}}) \tag{48}$$

while from the long-time side, substituting equation (47) into (30), we have

$$K_{0/1}(1) = \frac{1}{2}\left(1 \pm \frac{1}{1 + c\sqrt{1 + c^2} + c^2}\right) \tag{49}$$

introducing the shorthand $c = 8\pi\langle g \rangle$. These equations are consistent with one another if

$$\mathrm{e}^{-2\lambda t_{\mathrm{H}}} = \frac{1}{1 + c\sqrt{1 + c^2} + c^2} \tag{50}$$

or, resolving for c,

$$c = \frac{1 - \mathrm{e}^{-2\lambda t_{\mathrm{H}}}}{\sqrt{\mathrm{e}^{-2\lambda t_{\mathrm{H}}}(2 - \mathrm{e}^{-2\lambda t_{\mathrm{H}}})}}. \tag{51}$$

For $\lambda t_{\mathrm{H}} \ll 1$ (narrow connecting channel or weak coupling), proportionality $\langle g \rangle \approx \lambda t_{\mathrm{H}}/4\pi$ results. It represents a simple relation between the parameter of the quantum mechanical splitting distribution and the classical timescale of equilibration between the cells.

We state the full time dependence of the form factors in the long-time regime, again using the abbreviation c for the sake of conciseness,

$$K_{0/1}(\tau) = \frac{1}{2}\left(1 \pm \frac{1}{1 + c\tau\sqrt{1 + c^2\tau^2} + c^2\tau^2}\right). \tag{52}$$

In figures 4(*a*) and (*b*), we give a synopsis of $K_{0/1}(\tau)$ and $Y_{0/1}(r) = \int_0^\infty \mathrm{d}\tau\,[1 - K_{0/1}(\tau)]\cos(2\pi r\tau)$, respectively, for values of the decay constant ranging from $\lambda \ll 1$ to $\lambda \approx 1$. Figure 4 illustrates the crossover of the spectral two-point correlations from the regime of almost immediate equidistribution between the cells, $\lambda \gtrsim 1$, where the two-point statistics barely deviates from the corresponding Gaussian orthogonal ensemble (GOE) or Gaussian unitary ensemble (GUE) prediction (for figure 4, we have chosen the case of broken time-reversal invariance where the semiclassical approximation to the random-matrix form factor is exact), to the regime of weak coupling, $\lambda \ll 1$, with $K_0(\tau)$ rising to a marked peak near $\tau = 1$.

6. Models and numerical results

In the following sections, we introduce five quite diverse models that allow one to construct systems with two coupled compartments. The numerical results obtained for these models serve to illustrate and check various aspects of the theory developed above.

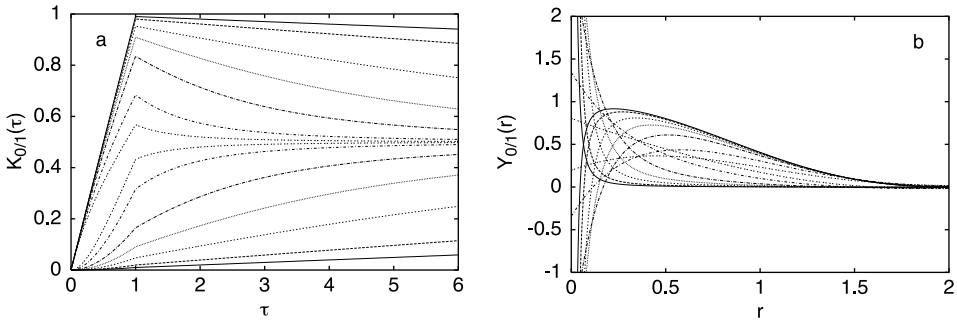

Figure 4. Group-element-specific form factors (*a*), as described by equations (23) and (52), and corresponding cluster functions (*b*), for the case of broken time-reversal invariance. (*a*) The upper curves show $K_0(\tau)$, the lower curves $K_1(\tau)$. (*b*) The graphs with positive initial slope correspond to $Y_0(r)$, those with negative initial slope to $Y_1(r)$. From the outmost to the innermost pair of curves, the decay rate takes the values $\lambda t_{\mathrm{H}} = 0.01, 0.02, 0.05, 0.1, 0.2, 0.5, 1.0$. Graphs of form factors and cluster functions for equal values of λt_{H} share a common line signature.

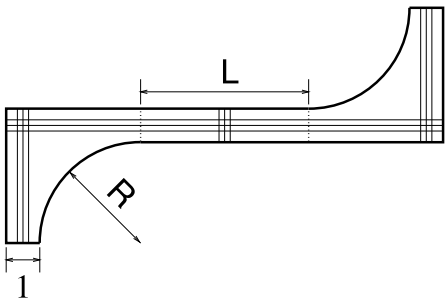

Figure 5. The Z-shaped billiard and the three different families of bouncing-ball orbits.

6.1. The Z-shaped billiard

We construct a two-cell billiard from two quarters of a Sinai billiard [19] and a straight channel such that the resulting shape resembles the letter Z [29] (figure 5). The width of this channel will serve as the basic length unit. The remaining parameters of the billiard are then the length L of the channel and the common radius R of the quarter-circle sections of the boundary.

Since the billiard boundary consists exclusively of defocusing and neutral components, the classical dynamics is ergodic and mixing [19]. Hence, we can assume that equation (2) holds to a good approximation, although for finite time systematic deviations from ergodicity, e.g., due to the presence of bouncing-ball orbits (figure 5), can be observed. In the following, we neglect such effects which have been studied in detail in [29].

The employed quantization scheme is described in appendix C. Figure 6 shows a representative example of a pair of eigenfunctions of the double billiard with quasidegenerate eigenenergies.

Figure 7 shows a comparison of the various form factors, as defined in section 3, with random-matrix theory. The energy was restricted by a rectangular window to the region $\pi < k < 5$, corresponding to one open channel in the connecting section of the billiard. In figure 7, we show the symmetry-projected form factors $\tilde{K}_+(\tau)$ ((*a*),(*b*)) and $\tilde{K}_-(\tau)$ ((*c*),(*d*)) (cf equation (12)), as well as the group-element-specific ones $K_0(\tau)$ ((*e*),(*f*)) and $K_1(\tau)$ ((*g*),(*h*)) (cf equation (14)), together with the corresponding predictions of random-matrix theory.

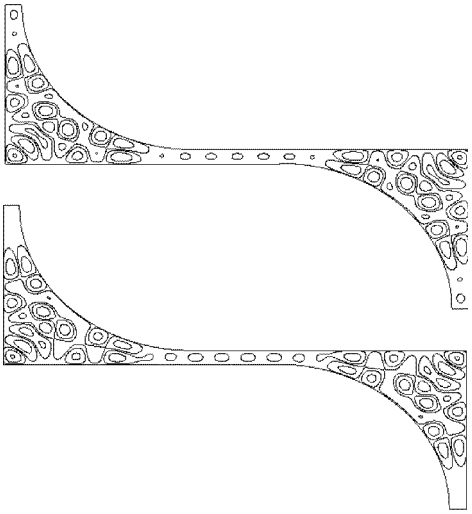

Figure 6. Contour plot of the absolute square of a pair of eigenfunctions of the double billiard with quasidegenerate energies. The state with even symmetry has $k = 3.7569$ (top), the antisymmetric state has $k = 3.7576$ (bottom). The geometric parameter values are $R = 10$ and $L = 5$.

The right-hand column contains blowups of the short-time regime of the data shown on the left. The $\tilde{K}_{\pm}(\tau)$ closely follow the GOE prediction for a single cell of the double billiard, as expected. For short times, $K_0(\tau)$ and $K_1(\tau)$ deviate significantly from the GOE shape, in the way predicted by semiclassical considerations. The initial slope of $K_0(\tau)$ is increased by a factor 2, while that of $K_1(\tau)$ vanishes. However, the amount of data obtained for this model is too small to allow for a quantitative comparison with the semiclassical theory beyond the vicinity of $\tau = 0$. Moreover, our numerical quantization procedure did not allow us to go to parameter values where $\lambda t_{\mathrm{H}} \lesssim 0.5$ such that $K_0(\tau)$ is expected to overshoot near $\tau = 1$. For the parameter values underlying the data shown, we have $\lambda t_{\mathrm{H}} \approx 4$, so that classical equilibration between the cells occurs around $\tau \approx 0.125$, cf equation (23).

6.2. The Sinai billiard

Another example of a two-cell billiard is provided by one half of the Sinai billiard as shown in figure 8. A semicircle of radius R divides a rectangle with side lengths L_x, L_y, into two parts connected by an opening of size $s = L_y - R$ along the symmetry axis. According to equation (5), the width of this constriction determines the classical rate of transitions between the two cells in the ergodic regime. The geometry of this billiard differs from that of the system discussed in the previous section in three respects: the single cells are no longer symmetric in themselves, there is no extra connecting channel of variable length, and the full configuration has reflection rather than inversion symmetry. The main advantage is, however, that there exists a more efficient quantization algorithm [20], again based on the scattering approach [27]. The reflection symmetry allows one to compute the eigenvalues in the two parity classes separately by requiring Neumann or Dirichlet boundary conditions along the symmetry axis. We unfold both spectra using the area and circumference contributions to the mean spectral density of one cell [30] and arrive at the scaled energy eigenvalues.

Our theory, developed in sections 2–5, is based on spectral two-point correlations that indiscriminately include *all* level pairs in the spectrum. The symmetry-based quantization

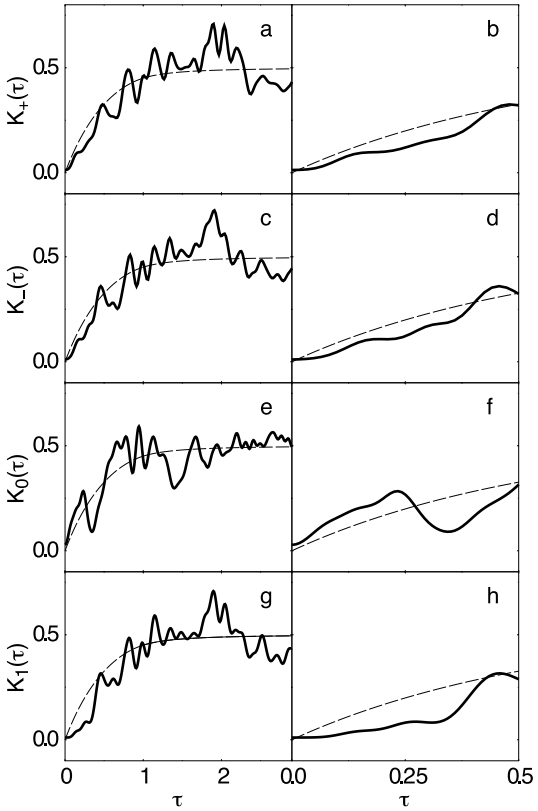

Figure 7. Time evolution of various form factors (heavy curves), compared with random-matrix theory (broken). The upper two rows show the symmetry-projected form factors ((*a*)–(*d*)), the lower ones the group-element-specific form factors ((*e*)–(*h*)). The right column consists of blowups of the short-time regime of the data shown on the left. The geometric parameter values are $R = 5$ and $\langle L \rangle = 6.7$.

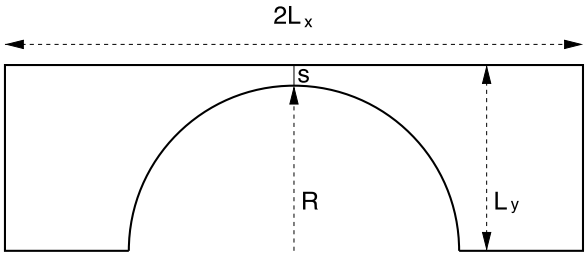

Figure 8. One half of the Sinai billiard consisting of a rectangle and an inscribed semicircle which divides the system into a reflection-symmetric pair of cells. The numerical data presented in this section correspond to $L_x = 2$, $L_y = 1$, and $s = 0.05$.

procedure used for the present model, by contrast, gives us immediate access to the scaled eigenvalues $r_{\alpha,\pm}$, presorted according to parity. We take this opportunity to make a few remarks concerning the 'genuine' doublets, i.e., level pairs with identical quantum number α but opposite symmetry, and their splittings $r_\alpha = r_{\alpha,-} - r_{\alpha,+}$. We emphasize again that only in the regime of small splittings, statistically independent of the positions of the doublet centres,

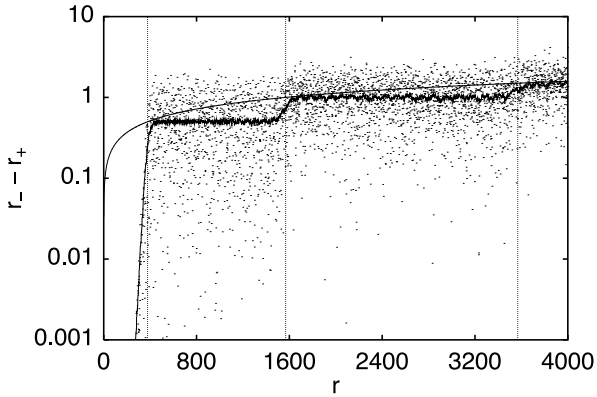

Figure 9. Spacings between pairs of unfolded energy eigenvalues with equal quantum number with respect to a single cell in figure 8 and Dirichlet/Neumann boundary conditions along the symmetry axis. The vertical lines mark the threshold energies where the first three quantum channels between the cells open. A running average of the spacings (wavy curve) is compared with the high-energy approximation (smooth curve).

does the two-point statistics embodied in the form factors coincide with the distribution of the genuine doublet splittings, cf equation (32). Outside this regime, the two-point statistics includes separations that are possibly very small but belong to states labelled by different quantum numbers, and therefore do not contribute to the splitting distribution. In effect, the two-point statistics is less restrictive and shows more weight at small separations than the splitting distribution.

Figure 9 shows the individual doublet splittings (dots) and a running average (wavy curve) as a function of the energy. We observe that the average splitting essentially depends on the number $\Lambda = [ks/\pi]$ of open quantum channels in the constriction. For low energy, quasidegenerate doublets prevail. In particular, below the threshold energy of the first quantum channel, we have $|\tilde{r}_\alpha| \ll 1$ for all pairs of eigenvalues. Because of the analogy with actual tunnel splittings [14], we presume that a semiclassical description of the spectrum in this regime should include also orbits with complex action including the diffractive orbits studied in [31]. This question will be investigated elsewhere.

As the energy approaches the opening of the first channel, the mean doublet splitting increases exponentially, and doublet splittings larger than the mean level spacing accumulate. Beyond the opening of the second quantum channel, even the average splitting exceeds the mean spacing. Consequently, for high energy, the notion of doublets becomes irrelevant for the spectral statistics of the composite system. It is, though, well suited in the regime of, e.g., a single open quantum channel, as we show below.

An approximation to the mean value of the doublet spacing is obtained from the asymptotic expansion of the mean spectral staircases $\bar{N}_\pm$ of the two subspectra. While the leading contribution depending on the area A is the same for both spectra, the second term depends on the circumference u and the boundary conditions. For $\hbar = 2m = 1$, we have

$$\bar{N}_-(E) = \frac{A}{4\pi}E - \frac{u}{4\pi}E^{1/2} \qquad \bar{N}_+(E) = \bar{N}_-(E) - \frac{s}{2\pi}E^{1/2}. \tag{53}$$

With the approximate quantization condition for scaled energy, $\bar{N}_\pm(E_{\alpha,\pm}) = \alpha + \frac{1}{2}$ [32], this leads to

$$|r_\alpha| \approx s\sqrt{r/A\pi} \tag{54}$$

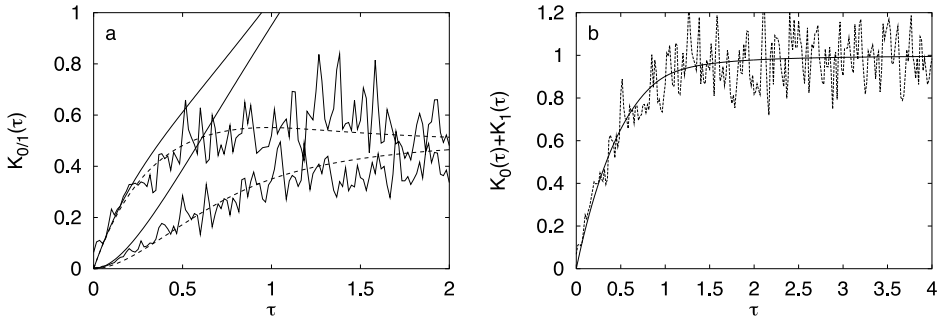

Figure 10. (*a*) Form factors $K_{0/1}(\tau)$ for the two-cell Sinai billiard of figure 8. The smooth solid curves represent the semiclassical result in diagonal approximation (23), the dashed lines show a fit to the ansatz (55) which explicitly obeys equation (16). The validity of the sum rule (16) is demonstrated in (*b*), where the solid curve represents the GOE form factor.

which is represented by a smooth solid curve in figure 9. We see that for low energy, the approximation (54) is correct only in the vicinity of the channel openings, while the mean splitting is approximately constant between the thresholds. Accordingly, taking the value predicted by equation (54) at the opening of the first channel $r = A\pi/4s^2$ for the entire subsequent interval until the next threshold, we find that the mean dimensionless doublet splitting for one open channel is $\frac{1}{2}$, independent of the size of the hole. Thus, it is already of the order of the mean level spacing of the composite two-cell system.

It is an important point that this does not restrict the applicability of our theory: the high probability of large doublet splittings corresponds to the fact that $p_{\mathrm{d}}(r)$, as obtained from equation (39), has a diverging first moment. Nevertheless, its Fourier transform is well behaved. Beyond the Heisenberg time, where we make use of it, it is essentially determined by the behaviour of the distribution at small spacings. Indeed, figure 9 shows a large number of doublets with a width well below the mean level spacing, which justifies our approach.

In figure 10(*a*), we present the form factors $K_{0/1}(\tau)$ obtained from the 1187 doublets with one open quantum channel. The size of this interval is a compromise between good statistics and the necessity to consider an energy interval in which the parameters entering the semiclassical description—notably the number of open channels and the classical decay constant—do not change appreciably. For the parameter λt_{H} entering the semiclassical theory we use the value obtained from equation (5) with k as at the centre of the considered interval. An effective averaging over τ was achieved by superimposing the form factors obtained after splitting the available spectrum into small pieces of 30 doublets each, with a rectangular window.

The dashed curve shows the prediction of the semiclassical diagonal approximation (23), which correctly describes the behaviour of the form factors for small τ, but fails close to the Heisenberg time $\tau = 1$ as discussed at the end of section 4 in connection with the sum rule (16). The validity of this relation is demonstrated in figure 10(*b*). It is interesting to note that all our data for systems with time-reversal invariance can be fitted very accurately (with λ as a free parameter) using an ansatz which combines (16) and the semiclassical result (23) into

$$K_{0/1}(\tau) = K_{\mathrm{RMT}}(\tau) P_{0/1}(\tau t_{\mathrm{H}}). \tag{55}$$

We cannot further substantiate this expression analytically.

Due to the poor outcome of the diagonal approximation in the present case, we cannot directly determine the mean resonance width from the decay constant by matching (23) and (30) at $\tau = 1$. Lacking a better semiclassical theory we fit $\langle g \rangle$ to our data, and we do so in

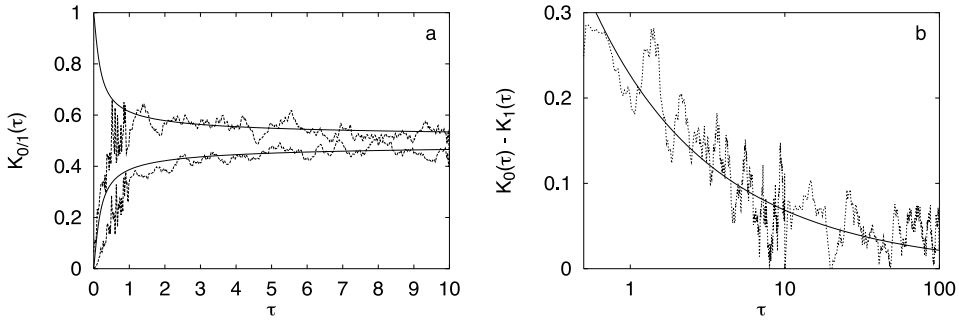

Figure 11. Long-time behaviour of the group-element-specific form factors for the two-cell Sinai billiard. (*a*) shows $K_{0/1}(\tau)$ together with the prediction according to equation (30). The parameter $\langle g \rangle$ was obtained by a fit to the short-time behaviour in the vicinity of the Heisenberg time $\tau = 1$ (see text). (*b*) shows the difference of the two form factors, which contains all essential information.

the vicinity of the Heisenberg time. For the fitting we have actually used the fact that (55), as shown in figure 10, represents our data up to and slightly beyond the Heisenberg time very well. $\langle g \rangle$ was determined as the value for which the long-time expression for the form factor matches smoothly to this ansatz. We prefer this procedure to a standard least-square fit over a large time interval, since it emphasizes that the value of $\langle g \rangle$ is at least implicitly contained in the *short-time* behaviour of the form factor.

With $\langle g \rangle$ obtained in this way, (30) describes $K_{0/1}(\tau \geqslant 1)$ very well (figure 10). Since the sum of the two form factors $K_0 + K_1$ is constant according to (16) and figure 10(*b*), all information is contained in the difference of the form factors which is shown in figure 11(*b*). We regard the good agreement over a very long time as numerical evidence in favour of the presented theory for the long-time behaviour of the form factor although it contains $\langle g \rangle$ as a fit parameter.

6.3. Quantum graphs

In this section we construct and investigate a two-cell system consisting of a quantized graph. It was recently shown [21] that quantum graphs exhibit the common quantum signatures of chaos and allow for a formally semiclassical description on the basis of non-deterministic classical dynamics.

A graph is defined by $v = 1, \ldots, V$ vertices and $2B$ directed bonds connecting them. The bond b with length L_b is understood to lead from vertex $v(b)$ to $v(\bar{b})$, $\bar{b}$ being the reversed bond ($L_{\bar{b}} = L_b$). On each bond we use a coordinate x_b with $x_b = 0$ at $v(b)$, $x_b = L_b$ at $v(\bar{b})$ and $x_{\bar{b}} = L_b - x_b$. The wavefunction $\phi_b(x_b)$ satisfies the Schrödinger equation ($\hbar = 2m = 1$)

$$\left(\left[\frac{\mathrm{d}}{\mathrm{d}x_b} \right]^2 + k^2 \right) \phi_b(x_b) = 0. \tag{56}$$

At the vertices, boundary conditions are chosen such that the current is conserved and the resulting Hamiltonian is self-adjoint and time-reversal invariant. Following the definitions in [21], we require (i) that the wavefunction is continuous across all vertices, i.e. it has the same value in all bonds b connected to some vertex v:

$$\phi_b(0) = \psi_{v=v(b)} \tag{57}$$

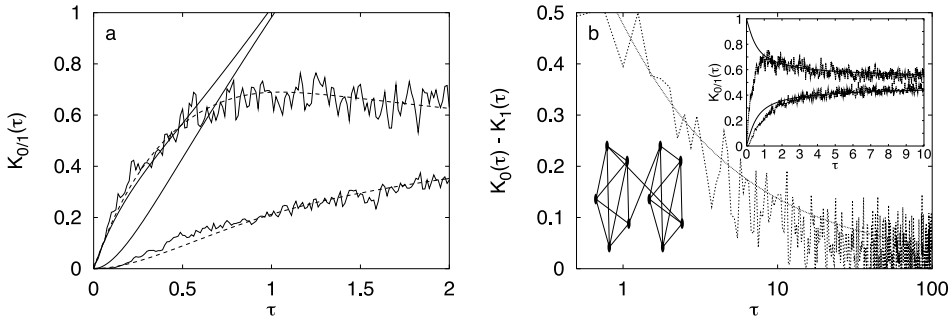

Figure 12. (*a*) Form factors $K_{0/1}(\tau)$ for the two-cell quantum graph compared with the semiclassical diagonal approximation and the ansatz (55) as in figure 10(*a*). (*b*) The difference of the form factors to the theory for the long-time behaviour with the parameter $\langle g \rangle$ obtained as in figure 11. The insets show the analogue of figure 11(*a*) and the topology of the unit cell.

and (ii), that the sum of the momenta in these bonds vanishes:

$$\sum_b \delta_{v,v(b)} \frac{\mathrm{d}}{\mathrm{d}x_b} \phi_b(0) = 0. \tag{58}$$

The eigenvalues of the so-defined graphs can easily be found numerically [21]. For the unit cell, we have interconnected $V = 10$ vertices using $B = 20$ bonds such that each vertex is the intersection of exactly four bonds (inset of figure 12(*b*)). In this case the classical dynamics is particularly simple: on the bonds, there is free motion at speed $2k$ and each vertex scatters the particle into any attached bond with equal probability $\frac{1}{4}$. On basis of such classical dynamics, a formally semiclassical quantization can be formulated which turns out to be exact in this model.

One of the bonds connecting the two pentagonal layers in figure 12(*b*) was sectioned, and both ends connected to a second identical unit cell, such that both cells form a ring with translation invariance in the direction 'normal' to the pentagonal layers. The bond lengths L_b of the unit cell are chosen as random numbers, such that the reflection symmetry is broken. The total length is normalized according to $\sum_b L_{b=1}^B = \pi$ so that the mean level spacing in k of the unit cell is unity. Therefore, it is advantageous to use the wavenumber k and the path length L, instead of energy and time, as conjugate variables for the semiclassical description. The Heisenberg time is thus replaced by the Heisenberg length $L_\mathrm{H} = 2\pi$ and dimensionless time is introduced as $\tau = L/L_\mathrm{H}$. In the ergodic regime, the escape rate from the unit cell (again with respect to unit path length instead of unit time) is simply given by the inverse total length of the graph, $\lambda = 1/\pi$.

It is a particularly favourable feature of the model that neither this rate nor the number of quantum channels connecting the two cells depend on energy. Therefore, we can average over arbitrarily large energy intervals. We have computed the form factor from the 10 000 lowest doublets after dividing the spectrum into groups of 40 doublets each, with a rectangular window function. Figure 12 compares the data as in the previous section with the diagonal approximation, the ansatz (55) and the long-time theory (41). The results correspond to those for the Sinai billiard but, due the larger amount of data, the agreement with our theoretical predictions is even closer.

6.4. The quantum kicked rotor on a torus

The kicked rotor belongs to the class of one-dimensional systems that are rendered classically chaotic only by a periodic driving. Its phase space is spanned by an angle and an angular-momentum variable and therefore has the topology of a cylinder. The nonlinearity of the potential is restricted to its time-dependent component and is controlled by a perturbation parameter. Accordingly, the classical dynamics crosses over smoothly from integrability to global chaos with increasing nonlinearity parameter, thereby following the KAM scenario [33, 34]. The phase space of the kicked rotor is also periodic with respect to its non-cyclic coordinate, namely along the angular-momentum axis.

Quantum mechanically, the classical angular-momentum period coexists with $\bar{h}$ as a second independent action scale. If both are commensurable, then the quantum kicked rotor is also periodic with respect to angular momentum and can serve as a model for solid-state-like systems with discrete spatial translation invariance. Since, in the periodic case, the cylindrical phase space may be regarded as being bent back on itself, this variant of the model is referred to as the 'kicked rotor on a torus'. It is this case which we shall discuss below. If the two angular-momentum periods are incommensurate, the quantum eigenstates are generally localized. In this case, the kicked rotor provides a model for Anderson localization in disordered systems [3, 22]. We will not consider it here.

The kicked rotor is defined by its Hamiltonian

$$H(l,\vartheta;t)=\frac{(l-\Lambda)^2}{2}+V_{\alpha,k}(\vartheta)\sum_{m=-\infty}^{\infty}\delta(t-m\tau). \tag{59}$$

As a consequence of the periodic time dependence, spectrum and eigenstates are adequately discussed in terms of quasienergies and Floquet states, respectively. In addition, the kicked rotor may possess two independent twofold antiunitary symmetries, both resembling time-reversal invariance. In order to break them in a controlled manner, an angular-momentum shift Λ has been introduced, and the potential is chosen as [35]

$$V_{\alpha,k}(\vartheta)=k\left[\cos\left(\alpha\frac{\pi}{2}\right)\cos\vartheta+\frac{1}{2}\sin\left(\alpha\frac{\pi}{2}\right)\sin 2\vartheta\right]. \tag{60}$$

Here, the global prefactor k determines the degree of nonlinearity. The appropriate classical measure of nonlinearity, however, is the parameter $K=k\tau$. If $K\gg 1$, chaotic motion prevails and angular momentum diffuses without restriction by KAM tori.

The ratio of the classical to the quantum period of action is determined by the parameter $\tau/4\pi$. If it is rational, i.e. if $\tau=4\pi p/q$ with p, q coprime, a unit cell along the angular-momentum axis arises that accommodates q quanta of angular momentum. The number of quasienergy levels per unit cell is then also q. We set $p=1$ and, in order to avoid an unwanted symmetry of the unit cell, require q to be odd.

According to Bloch's theorem, the spatial periodicity implies the existence of an additional constant of the motion, the Bloch phase θ. It appears explicitly in the symmetry-projected Floquet operator [22],

$$\langle l'|\hat{U}(\theta)|l\rangle=\exp\left(-2\pi\mathrm{i}\frac{p}{q}(l-\Lambda)^2\right)\frac{1}{q}\sum_{n=0}^{q-1}\mathrm{e}^{-\mathrm{i}V_{\alpha,k}([\theta+2\pi n]/q)}\mathrm{e}^{\mathrm{i}(l-l')(\theta+2\pi n)/q}. \tag{61}$$

A restriction of the lattice to a finite number of N unit cells, with cyclic boundary conditions at the ends, amounts to discretizing the Brillouin zone so that it comprises N equidistant values $\theta_m=2\pi m/N$, $m=0,\ldots,N-1$, of the Bloch phase. The independent parameter N corresponds to the number of levels per band; the total number of levels in the spectrum is Nq.

A system with two unit cells is simply constructed by setting $N = 2$. In contrast to the systems discussed above, the resulting model does not possess a bottleneck between its two compartments, neither in configuration space nor in phase space. A reduced exchange between them therefore comes about solely by slow diffusion. The exchange rate λ is determined by the diffusion constant $D = k^2/2$ (valid if $K \gg 1$) through the simple relation $\lambda = D/(2a^2)$ derived in appendix A. In the quantum kicked rotor on a torus, the integer q represents the dimensionless size of the unit cell, to be substituted for a.

The most interesting parameter regime to be studied numerically would be one where $K_0(\tau)$ exhibits a positive peak around $\tau = 1$, the feature indicating quasidegeneracy in the spectrum. For this peak to emerge, the exchange between the cells must be slow. Since there is no bottleneck in the kicked rotor, this can only be achieved through a small diffusion constant. More precisely, it requires that the Heisenberg time should be small against the Thouless time. Measured in units of the discrete time steps of the kicked rotor they are, respectively, $n_{\mathrm{H}} = q$ and $n_{\mathrm{D}} = N^2q^2/(\pi D)$, so that the condition for quasidegeneracy to occur reads

$$N^2 \gg \frac{\pi k^2}{2q}. \tag{62}$$

At the same time, it should be avoided that localization becomes effective even within the unit cells, in order to separate the signature of classical diffusion from the direct quantal effect of disorder in the spectrum. The localization length should therefore be kept large compared with the size of the unit cell,

$$\xi \approx \frac{k^2}{4} \gg q. \tag{63}$$

Clearly, both conditions, (62) and (63), can hardly be met simultaneously if N is fixed and small. With $N = 2$, little freedom remains since, in addition, being close to the classical limit and well within the classically chaotic regime requires both q and k to be large. We found that $q = 45$ and $k = 10$ represents an acceptable compromise. The resulting diffusion constant, corrected for oscillations occurring if $K \gtrsim 1$ [33], is $D = 23.23$. We substitute the Thouless time $\tau_{\mathrm{D}} = n_{\mathrm{D}}/q = 2.467$ for the time constant $1/(\lambda t_{\mathrm{H}})$ of the exponential equilibration.

Form factors have been computed, according to equations (9) and (11), using cosine-shaped windows ($\chi(x) \sim 1 + \cos x$ if $|x| \leqslant \pi$) of width $2\pi/M$, with $M = 9$, each one comprising of the order of $qN/M = 10$ quasienergy levels. For a general account of spectral two-point statistics in periodically driven systems with quasienergy spectrum, see appendix A in [3].

In figures 13(*a*) and (*b*), we compare the form factors $K_{0/1}(\tau)$ and corresponding cluster functions $Y_{0/1}(r)$, respectively, obtained for the quantum kicked rotor on a torus with parameters as above, with our theory according to equations (23) and (52). For the evaluation of the theory, we have used the relations cited to determine the decay rate directly from q and k. *No fitting was involved.* The data cover ten Heisenberg times and thus reach far into the quantum long-time regime. In the form factors, we can clearly discern the three time domains discussed: the initial phase of chaotic diffusion where $K_0(\tau)$ is strongly enhanced while $K_1(\tau)$ remains close to zero, the sharp positive peak of $K_0(\tau)$, reaching almost twice the asymptotic value, and the saturation regime where $K_0(\tau)$ and $K_1(\tau)$ approach their common asymptote from above and below, respectively. The cluster function for $r \lesssim 1$ represents the regime of long times or small splittings in a different manner. Both plots give evidence that the theory provides a quantitative description of the two-point correlations over all time/energy scales.

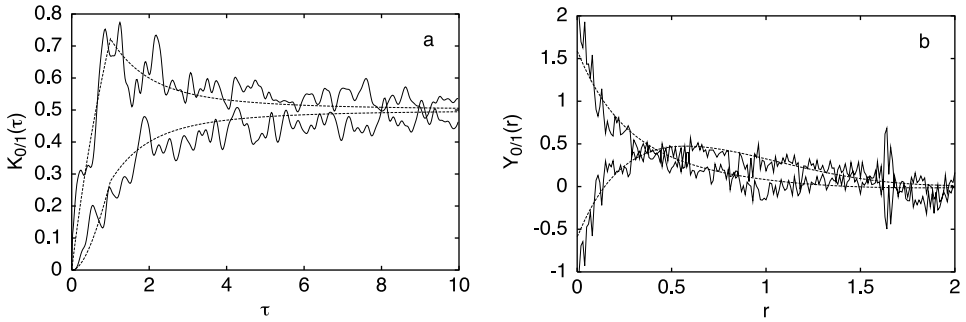

Figure 13. (*a*) Group-element-specific form factors as described by equations (23) and (52). (*b*) Corresponding cluster functions for the quantum kicked rotor on a torus, compared with the theory according to equations (23) and (52) (dashed curves). The parameter values are $q = 45$ and $k = 10$, corresponding to an exchange rate $\lambda = 0.258$.

6.5. A random-matrix model

In this section, we consider a simple model for a reflection-symmetric double-well system with chaotic dynamics, with and without time-reversal symmetry, constructed in the spirit of [11, 12]. It is shown that in certain cases, this model qualitatively reproduces the features of the form factor discussed in sections 4 and 5.

We consider a Hamiltonian of the form

$$H = \begin{pmatrix} H_0 & V \\ V & H_0 \end{pmatrix} \tag{64}$$

where H_0 represents the internal dynamics of either cell in an N-dimensional Hilbert space, and V their coupling via $M \ll N$ channels of the connecting duct. Note that in contrast to the models discussed in [9, 11, 12], we require the two blocks on the diagonal to be identical.

We model H_0 as an $N \times N$ random matrix distributed according to Dyson's Gaussian ensembles, $P(H_0)\,\mathrm{d}H_0 \propto \exp(-\operatorname{Tr} H_0^2/4)\,\mathrm{d}H_0$. It is assumed that $N \to \infty$. The $N \times N$ matrix V has the form

$$V_{kl} = \delta_{kl}\frac{N}{M}\frac{v\Delta}{\pi^2} \qquad \text{for} \quad k = 1, \ldots, M \tag{65}$$

and zero for $k > M$. Here, $M \ll N$ is the number of matrix elements coupling the two wells, v parametrizes their strength, and Δ is the mean level spacing of H_0, $\Delta = \pi\sqrt{\beta/N}$ with $\beta = 1$ in the GOE and $\beta = 2$ in the GUE.

The Hamiltonian H has a twofold symmetry. Its eigenvalues can be classified according to parity p and appear as doublets $r_{\alpha,\nu}$ with $\alpha = 1, \ldots, N$ and $\nu = \pm$. According to equation (28), we write $r_{\alpha,\pm} = R_\alpha \pm r_\alpha$. The form factor is then given by (cf equation (29))

$$K_{0/1}(\tau) = \frac{1}{2} \pm \left\langle \frac{1}{2N}\sum_{\alpha=1}^{N} \cos(4\pi\tau r_\alpha) \right\rangle. \tag{66}$$

For large times ($\tau \gg 1$), $K_{0/1}(\tau)$ may be calculated by evaluating the doublet splitting $2r_\alpha$ within degenerate perturbation theory. Denoting the eigenfunctions of H_0 by ϕ_α (with components $\phi_{\alpha\nu}$), one has (with $\langle d_{\mathrm{fd}}\rangle = \Delta^{-1}$)

$$r_\alpha \simeq \frac{v}{\pi^2}\frac{N}{M}\sum_{\nu=1}^{M} |\phi_{\alpha\nu}|^2. \tag{67}$$

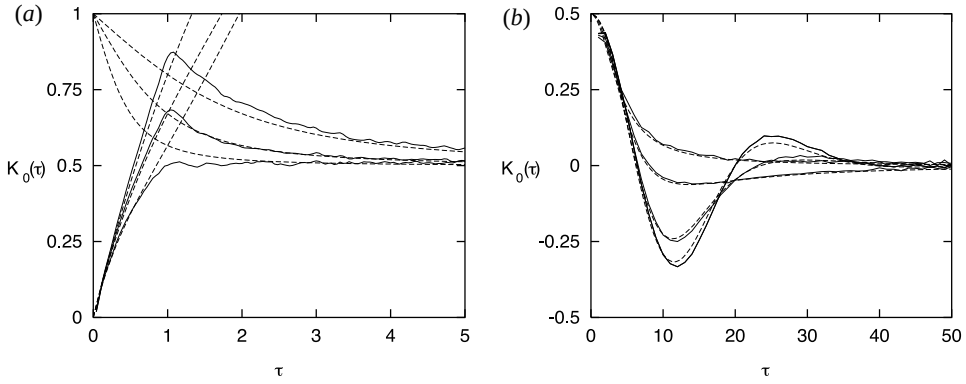

Figure 14. (*a*) Form factor $K_0(\tau)$ in the GUE for three different values of the coupling strength ($v = 0.5$, 1, and 2), and for $N = 80$ and $M = 1$ (full curves). Also shown are the theoretical results, equations (23) and (52) (dashed curves). (*b*) Form factor $K_0(\tau) - \frac{1}{2}$ in the GUE for $v = 0.2$, $N = 80$ and $M = 1$, 2, 6, and 10 (full curves), compared to the asymptotic theoretical result, equation (71) (dashed curves).

Substituting (67) into (66), it remains to average over the eigenfunctions ϕ_α of H_0. The statistical properties of the eigenfunctions ϕ_α depend on the ensemble considered. In the GUE, the amplitude $u = N|\phi_{\alpha\nu}|^2$ is distributed according to $P(u) = \exp(-u)$. In the GOE, the corresponding distribution is $P(u) = (2\pi u)^{-1/2}\exp(-u/2)$.

We first consider the case $M = 1$, where the two wells are coupled via a single matrix element. For $\tau \gg 1$, one obtains for $K_{0/1}(\tau)$

$$K_{0/1}(\tau) \approx \tfrac{1}{2} \pm \tfrac{1}{2} \begin{cases} \frac{1}{4}(v\tau/\pi)^{-1/2} & \text{for} \quad \beta = 1 \\ 1/[1 + (4v\tau/\pi)^2] & \text{for} \quad \beta = 2. \end{cases} \tag{68}$$

For $\beta = 1$, this expression reproduces the long-time $\tau^{-1/2}$ decay of equation (44). For $\beta = 2$, equation (68) reproduces the τ^{-2} decay for large τ implied by equation (47).

For $\beta = 2$, the matching procedure discussed in section 5 yields an analytical expression for $K_0(\tau)$ valid for all timescales. In figure 14(*a*), we compare this expression (equations (23), (52)) with results of simulations of the model (64). Shown is $K_0(\tau)$ as a function of τ for an ensemble of random matrices with $N = 80$, $v = 0.5$, 1 and 2 in the GUE (full curves), as well as equations (23) and (52). The constant v may be determined from $\langle g \rangle$ by comparison of equation (68) with (52), where $c = 8\pi\langle g \rangle$.

We find good agreement between the results of the simulations and equations (23), (52). We have, however, not attempted to evaluate the small-τ behaviour of the form factor for the model (64) analytically. For large τ, on the other hand, it is clear that equation (64) is a good model for the form factor: as pointed out above, equations (68) and (52) coincide for large τ.

In the present model, it is also possible to consider larger M, $1 < M \ll N$. In this case, for $\beta = 2$, the quantity

$$u = \frac{N}{M}\sum_{\nu=1}^{M} |\phi_{\alpha\nu}|^2 \tag{69}$$

is distributed according to

$$P(u, M) = \frac{M^M u^{M-1} \mathrm{e}^{-Mu}}{\Gamma(M)}. \tag{70}$$

We require $M \ll N$ since, for $M = N$, one has $u = 1$ due to normalization of the wavefunctions. In the GUE, the form factor is then given by

$$K_0(\tau) \approx \frac{1}{2} + \frac{1}{2}\int_0^\infty \mathrm{d}u \cos\left(\frac{4v}{\pi}\tau u\right) P(u, M)$$
$$= \frac{1}{2} + \frac{1}{2}\left(1 + \left(\frac{4v\tau}{\pi M}\right)^2\right)^{-M/2} \cos\left(M \arctan\left(\frac{4v\tau}{\pi M}\right)\right). \tag{71}$$

For $M = 1$, equation (68) is reproduced. For $1 < M \ll N$, the form factor does not decay monotonically for $\tau > 1$ but exhibits oscillatory behaviour (figure 14(*b*)).

7. Conclusion

Chaotic systems with two weakly connected cells, elementary as this concept may appear, form a paradigm for a large class of physical situations and exhibit a surprisingly rich behaviour. In this paper, we have shown that it is essentially determined by two parameters. One of them can be identified with the time required for the respective populations of the cells to equilibrate. It specifies the position between the extreme of a large opening that hardly restricts the exchange, and the opposite one of two almost isolated single cells. The second relevant parameter is a measure of the difference in shape between the cells, ranging from exact symmetry to its complete absence.

On the basis of the results obtained in this paper, we can draw a clear picture of the spectral two-point correlations in this two-dimensional parameter space. In the case of an effective communication between the cells, the presence or absence of symmetry is of little relevance for the spectral statistics. It is then only the slight retardation of ergodic coverage that becomes manifest in the level correlations. The result is a reduction in the area enclosed by the initial minimum (correlation hole) of the form factor, indicating an increase of randomness in the spectrum which can be completely accounted for by semiclassical considerations [5].

The case of two almost isolated cells lacking all symmetry can be trivially understood from a random-matrix point of view. We are then dealing with the superposition of two spectra that are nearly mutually independent but exhibit the same statistics. Here, random-matrix theory simply predicts a doubling of the time argument of the form factor [26], in agreement with the semiclassical approximation in the limit of slow equilibration.

If, in contrast, the two cells are symmetric, the formation of doublets introduces an additional feature in the spectrum. The corresponding positive correlations are reflected in the form factor as a maximum in the vicinity of the Heisenberg time. In the limit of long exchange time, the form factor at this maximum reaches twice the asymptotic value to which it decays subsequently from above, relative to its value at $t = 0$. In the case of exact symmetry, we can quantitatively account for this peak in the standard form factor. Simultaneously, there is a depression in an analogous statistic that refers to transport from one cell to the other, rather than to return to the initial one.

The crossover from full to completely broken symmetry, as a function of some symmetry-breaking parameter, can be included in the semiclassical theory if a few plausible additional assumptions are made. In accordance with corresponding work on spatially periodic systems with slight disorder [36], this approach implies that the peak in the form factor should decay exponentially both with the typical difference in action between symmetry-related periodic orbits in the respective cells, and with time.

Acknowledgments

TD would like to express thanks for the warm hospitality enjoyed during a stay with the group of Professor O Bohigas, at the Institut de Physique Nucléaire, Orsay. This stay was financed by Deutsche Forschungsgemeinschaft (grant no Di 511/4-1). BM gratefully acknowledges financial support by the *Sonderforschungsbereich 393 'Numerische Simulation auf massiv parallelen Rechnern'* of the DFG.

Appendix A. Discrete diffusion

The picture of a two-cell system with the topology of a ring suggests to unroll the ring so that an infinite chain is formed. If the two cells are translation symmetric, then each of them represents a unit cell of this periodic lattice, otherwise the unit cell comprises both cells of the ring. In this extended topology, the condition of slow exchange between the cells implies that the picture of homogeneous diffusion breaks down on the scale of the lattice constant. We are therefore in a regime opposite to that considered in [1].

The spreading along the chain is now determined by a master equation for the probability to be at site n, instead of a diffusion equation for the probability density,

$$\dot{P}_n(t) = \lambda P_{n-1}(t) - 2\lambda P_n(t) + \lambda P_{n+1}(t). \tag{A.1}$$

In a more concise notation, it reads

$$\left(\frac{\mathrm{d}}{\mathrm{d}t} - \lambda\Delta_2\right)\boldsymbol{P}(t) = 0. \tag{A.2}$$

Here, $\boldsymbol{P}(t)$ denotes the entire infinite vector of the $P_n(t)$, and

$$\Delta_2 = \begin{pmatrix} \cdot & \cdot & \cdot & & & & & \\ & \cdot & \cdot & 1 & & & & 0 \\ & & 1 & -2 & 1 & & & \\ & & & 1 & -2 & 1 & & \\ & & & & 1 & -2 & 1 & \\ & 0 & & & & 1 & \cdot & \cdot \\ & & & & & & \cdot & \cdot & \cdot \end{pmatrix} \tag{A.3}$$

is the discrete Laplace operator. The lattice plane waves

$$\phi_{m,n} = \frac{1}{\sqrt{N}}\mathrm{e}^{2\pi\mathrm{i}nm/N} \qquad m = 0, \ldots, N-1 \tag{A.4}$$

where for the sake of normalizability we have reintroduced cyclic boundary conditions with a period of N chain elements, solve the stationary eigenvalue equation

$$\Delta_2\phi_m = \gamma_m\phi_m \tag{A.5}$$

with eigenvalues

$$\gamma_m = 2\left(\cos\frac{2\pi m}{N} - 1\right). \tag{A.6}$$

For a localized initial state

$$P_n(0) = \delta_{n \bmod N} = \frac{1}{\sqrt{N}}\sum_{m=0}^{N-1}\phi_{m,n} \tag{A.7}$$

the time evolution reads

$$P_n(t) = \frac{1}{\sqrt{N}} \sum_{m=0}^{N-1} \phi_{m,n} \mathrm{e}^{\gamma_m t}$$
$$= \frac{1}{N} \sum_{m=0}^{N-1} \exp\left(2\pi \mathrm{i} \frac{mn}{N} + 2\lambda \left[\cos\frac{2\pi m}{N} - 1\right] t\right). \tag{A.8}$$

By Poisson resummation, this becomes

$$P_n(t) = \frac{1}{N} \sum_{m=-\infty}^{\infty} \int_0^N \mathrm{d}\nu \, \exp\left(2\pi \mathrm{i}\left[m + \frac{n}{N}\right]\nu + 2\lambda\left[\cos\frac{2\pi\nu}{N} - 1\right] t\right)$$
$$= \mathrm{e}^{-2\lambda t} \sum_{m=-\infty}^{\infty} I_{|n+mN|}(2\lambda t) \tag{A.9}$$

where $I_n(z)$ denotes the modified Bessel function of integer order n [37]. The spreading over the lattice, as described by $P_n(t)$, represents a discrete diffusion process. If we go to the continuum limit by defining $x = na$, $L = Na$, and letting the lattice constant $a \to 0$, we recover continuous diffusion with periodic boundary conditions,

$$p(x,t) = \frac{1}{a} P_n(t) \to \frac{1}{\sqrt{2\pi Dt}} \sum_{m=-\infty}^{\infty} \exp\left(-\frac{(x+mL)^2}{2Dt}\right). \tag{A.10}$$

The diffusion constant is $D = 2\lambda a^2$. In performing the limit, we have used the asymptotic form of the $I_n(z)$ for large argument z [38] and expanded it for large order n. The two-cell solution, equation (2), is retained by setting $N = 2$ in equation (A.8).

Appendix B. Doublets as discretized bands

As on the level of the classical dynamics, it is instructive to also consider the quantum two-cell system as the unit cell of an infinite chain. From this point of view, the doublets $r_{\alpha,\pm}$ come about by discretizing continuous bands to a 'Brillouin zone' with only two points. The simplest possible interpolation between these points assumes cosine-shaped bands,

$$r_\alpha(\mu) = R_\alpha + r_\alpha \cos(\pi\mu) \qquad \mu = 0, 1. \tag{B.1}$$

Equation (B.1) can be justified by the fact that it imposes no more information on the shape of the bands than is available, namely their first two Fourier coefficients. Cosine-shaped bands result also from diagonalizing a tight-binding Hamiltonian with translation invariance. For two sites this is

$$H^{(\alpha)}_{n,n'} = R_\alpha \delta_{(n-n') \bmod 2} + \tfrac{1}{2} r_\alpha (\delta_{(n-n'-1) \bmod 2} + \delta_{(n-n'+1) \bmod 2}) \qquad n, n' = 0, 1. \tag{B.2}$$

We have defined the parameters of this Hamiltonian in such a way that equation (B.1) gives its eigenenergies. Inserting them in equation (27) and performing a Poisson resummation results in

$$a_n(\tau) = \sum_{m=-\infty}^{\infty} \sum_{\alpha=1}^{N_\mathrm{d}} \mathrm{e}^{-2\pi \mathrm{i} \tau R_\alpha} \mathrm{i}^{n-2m} J_{2m-n}(2\pi\tau r_\alpha) \tag{B.3}$$

where $J_k(z)$ denotes the ordinary Bessel function of order k. We introduce a diagonal approximation with respect to the band index α, as in section 5, and obtain the corresponding form factors as

$$K_n(\tau) = \frac{1}{N_\mathrm{d}} \sum_{\alpha=1}^{N_\mathrm{d}} \left| \sum_{m=-\infty}^{\infty} (-1)^m J_{2m-n}(2\pi\tau r_\alpha) \right|^2. \tag{B.4}$$

Invoking the sum rules $\sum_{k=-\infty}^{\infty}(-1)^k J_{2k}(z) = \cos z$, $\sum_{k=-\infty}^{\infty}(-1)^k J_{2k-1}(z) = \sin z$ [39], we recover equation (29).

Appendix C. Quantization of the Z-shaped billiard

Quantization of a billiard amounts to solving the Helmholtz equation

$$\left(\frac{\partial^2}{\partial x^2} + \frac{\partial^2}{\partial y^2} + k^2\right)\psi(x, y) = 0 \tag{C.1}$$

with Dirichlet boundary conditions on the billiard circumference and a dispersion $k^2 = 2mE/\hbar^2$. In this appendix we describe a specific quantization method for the Z-shaped billiard discussed in section 6.1. It is based on the scattering approach [20,27]. Consider a subdivision of the closed double billiard into two open halves (figure 2). Each of them represents a chaotic scatterer attached to the end of a semi-infinite waveguide. Within the waveguide, quantization of transverse momentum, $k_{y,n} = n\pi$, $n = 0, \pm 1, \pm 2, \ldots$, implies that there are $N = [k/\pi]$ ([...] denoting integer part) open channels with real longitudinal momentum $k_{x,n} = (k^2 - k_{y,n}^2)^{1/2}$, such that the two scatterers are described by $N \times N$ scattering matrices S^{l} and S^{r}, respectively.

The secular equation for the eigenvalues of the full billiard then reads

$$\det(I - S^{\mathrm{l}}(k)S^{\mathrm{r}}(k)) = 0. \tag{C.2}$$

In order to construct the $S^{\mathrm{l/r}}$ for the billiard halves [27], we start from the $2N \times 2N$ transfer matrix for a quarter Sinai billiard open on both sides [2,3],

$$T^{\mathrm{s}} = \begin{pmatrix} rt^{-1}r - t & rt^{-1} \\ t^{-1}r & t^{-1} \end{pmatrix}. \tag{C.3}$$

Here, t and r denote the $N \times N$ matrices of transmission and reflection amplitudes, respectively. Due to the spatial reflection symmetry with respect to the diagonal, the two entrances of the billiard are equivalent.

The transfer matrix T^{w} for a waveguide of length $L/2$ consists of phase factors $\exp(\pm \mathrm{i}k_{x,n}L/2)$ along the diagonal. The letter-Z-like fashion in which the two halves are assembled is accounted for by a third factor T^{z} with appropriate phases ± 1 [2,3] along its diagonal. It is included in the transfer matrix for one of the sides, e.g., $T^{\mathrm{l}} = T^{\mathrm{e}}T^{\mathrm{w}}$, $T^{\mathrm{r}} = T^{\mathrm{l}}T^{\mathrm{z}}$.

The scattering matrices for the billiard halves closed on one side are obtained from T^{l} and T^{r} by requiring incoming and outgoing amplitudes to cancel across the openings where Dirichlet boundary conditions are to be enforced,

$$\begin{pmatrix} +\boldsymbol{A} \\ -\boldsymbol{A} \end{pmatrix} = T^{\mathrm{l/r}} \begin{pmatrix} \boldsymbol{B} \\ \boldsymbol{C} \end{pmatrix}. \tag{C.4}$$

Here, $\boldsymbol{A}$ and $-\boldsymbol{A}$ refer to the amplitudes at the ends to be closed, and $\boldsymbol{B}$ and $\boldsymbol{C}$ to the amplitudes on the opposite sides. The latter are related by $\boldsymbol{C} = S^{\mathrm{l/r}}\boldsymbol{B}$, invoking the S matrices sought after. Solving for them, one finds

$$S^{\mathrm{l/r}} = -(T_{12}^{\mathrm{l/r}} + T_{22}^{\mathrm{l/r}})^{-1}(T_{11}^{\mathrm{l/r}} + T_{21}^{\mathrm{l/r}}). \tag{C.5}$$

In obvious notation, $T_{ij}^{\mathrm{l/r}}$, $i, j = 1, 2$, refer to the four $N \times N$ subblocks of the respective transfer matrices.

In order to check the quality of the quantization procedure, we compare, in figure C1, the numerical result for the cumulated eigenvalue density with the Brownell formula [30], for wavenumbers in the interval $\pi < k < 2\pi$, and $R = 10$. The agreement is satisfactory up to

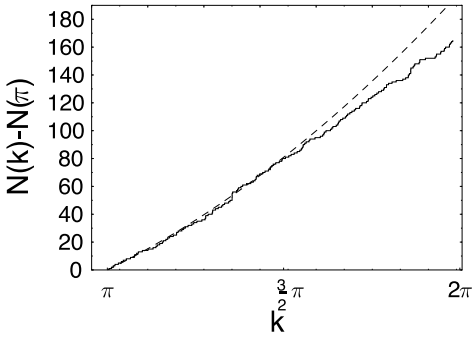

Figure C1. The cumulated eigenvalue density of the double billiard (steps) compared with the Brownell formula (dashed curve). The geometric parameter values are $R = 10$ and $L = 10$.

$k \approx 5$. For larger wavenumbers, quasidegenerate pairs of zeros occur in the secular function with spacings too small to be resolved by the numerical procedure. We have therefore discarded data with $k > 5$. To achieve better statistics in the evaluation of spectral correlations, we have varied L within an interval ΔL amounting to a few per cent of L.

References

[1] Dittrich T, Mehlig B, Schanz H and Smilansky U 1997 *Chaos Solitons Fractals* **8** 1205
Dittrich T, Mehlig B, Schanz H and Smilansky U 1998 *Phys. Rev.* E **57** 359
[2] Dittrich T and Smilansky U 1991 *Nonlinearity* **4**85
Dittrich T, Doron E and Smilansky U 1994 *J. Phys. A: Math. Gen.* **27** 79
[3] Dittrich T 1996 *Phys. Rep.* **271** 267
[4] Argaman N, Imry Y and Smilansky U 1993 *Phys. Rev.* B **47** 4440
[5] Smilansky U, Tomsovic S and Bohigas O 1992 *J. Phys. A: Math. Gen.* **25** 3261
[6] Campos D and Urbina J D to be published
[7] de Leon N and Berne B J 1982 *Chem. Phys. Lett.* **93** 169
[8] Brack M and Bhaduri R K 1987 Semiclassical physics *Frontiers in Physics* vol 96 (Reading, MA: Addison-Wesley) section 8.1 and references therein
[9] Alt H, Barbosa C I, Gräf H-D, Guhr T, Harney H L, Hofferbert R, Rehfeld H and Richter A 1998 *Phys. Rev. Lett.* **81** 4847
[10] Bohigas O, Tomsovic S and Ullmo D 1990 *Phys. Rev. Lett.* **64** 1479
Bohigas O, Tomsovic S and Ullmo D 1990 *Phys. Rev. Lett.* **65** 5
[11] Bohigas O, Tomsovic S and Ullmo D 1993 *Phys. Rep.* **223** 43
[12] Tomsovic S and Ullmo D 1994 *Phys. Rev.* E **50** 145
[13] Utermann R, Dittrich T and Hänggi P 1994 *Physica* B **194-196** 1013
Utermann R, Dittrich T and Hänggi P 1994 *Phys. Rev.* E **49** 273
[14] Creagh S C and Whelan N D 1996 *Phys. Rev. Lett.* **77** 4975
[15] Leyvraz F and Ullmo D 1996 *J. Phys. A: Math. Gen.* **29** 2529
[16] Lebœuf P and Mouchet A 1994 *Phys. Rev. Lett.* **73** 1360
[17] Hannay J H and Ozorio de Almeida A M 1984 *J. Phys. A: Math. Gen.* **17** 3429
[18] Berry M V 1985 *Proc. R. Soc.* A **400** 229
[19] Sinai Y G 1963 *Sov. Math. Dokl.* **4** 1818
Sinai Y G 1970 *Russ. Math. Surv.* **25** 137
[20] Schanz H and Smilansky U 1995 *Chaos Solitons Fractals* **5** 1289
Schanz H 1997 Investigation of two quantum chaotic systems *PhD Thesis* Logos, Berlin
[21] Kottos T and Smilansky U 1997 *Phys. Rev. Lett.* **79** 4794
[22] Izrailev F M 1990 *Phys. Rep.* **196** 299
[23] Bauer W and Bertsch G F 1990 *Phys. Rev. Lett.* **65** 2213
[24] Tinkham M 1964 *Group Theory and Quantum Mechanics* (New York: MacGraw-Hill)
[25] Robbins J M 1989 *Phys. Rev.* A **44** 2128
[26] Bohigas O 1992 *Chaos and Quantum Physics (Les Houches Lectures LII)* ed M-J Giannoni, A Voros and J Zinn-Justin J (Amsterdam: North-Holland) p 87
[27] Doron E, Smilansky U and Frenkel A 1991 *Physica* D **50** 367

Doron E and Smilansky U 1992 *Nonlinearity* **5** 1055
[28] Brody T A, Flores J, French J B, Mello P A, Pandey A and Wong S S M 1981 *Rev. Mod. Phys.* **53** 385
[29] Koboldt G 1997 *Diploma Thesis* University of Augsburg, unpublished
[30] Baltes H P and Hilf E R 1976 *Spectra of Finite Systems* (Zürich: Bibliographisches Institut)
[31] Primack H, Schanz H, Smilansky U and Ussishkin I 1996 *Phys. Rev. Lett.* **76** 1615
Primack H, Schanz H, Smilansky U and Ussishkin I 1997 *J. Phys. A: Math. Gen.* **30** 6693
[32] Aurich R, Matthies C, Sieber M and Steiner F 1992 *Phys. Rev. Lett.* **68** 1629
[33] Lichtenberg A J and Lieberman M A 1983 *Regular and stochastic motion (Applied Mathematical Sciences, vol 380)* (New York: Springer)
[34] Chirikov B V 1979 *Phys. Rep.* **52** 263
[35] Blümel R and Smilansky U 1992 *Phys. Rev. Lett.* **69** 217
Thaha M, Blümel R and Smilansky U 1993 *Phys. Rev.* E **48** 1764
[36] Dittrich T, Mehlig B, Schanz H, Smilansky U, Pollner P and Vattay G 1999 *Phys. Rev.* E **59** 6541
(Dittrich T, Mehlig B, Schanz H, Smilansky U, Pollner P and Vattay G 1998 *Preprint* cond-mat/9811322)
[37] Abramowitz M and Stegun I A 1984 *Pocketbook of Mathematical Functions* (Thun: Harri Deutsch) p 118
[38] Abramowitz M and Stegun I A 1984 *Pocketbook of Mathematical Functions* (Thun: Harri Deutsch) p 121
[39] Abramowitz M and Stegun I A 1984 *Pocketbook of Mathematical Functions* (Thun: Harri Deutsch) p 187